REPORT DOCUMENTATION PAGE

Form Approved
OMB No. 0704-0188

1. AGENCY USE ONLY (Leave blank)	2. REPORT DATE	3. REPORT TYPE AND DATES COVERED
	7/15/1991	Final Report 5/1/88-4/30/91

4. TITLE AND SUBTITLE

Time Domain Electromagnetic Waves in Multilayered Media

5. FUNDING NUMBERS

DAAL03-88-K-0057

6. AUTHOR(S)

J. A. Kong

7. PERFORMING ORGANIZATION NAME(S) AND ADDRESS(ES)

Center for Electromagnetic Theory and Applications
Research Laboratory of Electronics
Massachusetts Institute of Technology
Cambridge, MA 02139

8. PERFORMING ORGANIZATION REPORT NUMBER

9. SPONSORING/MONITORING AGENCY NAME(S) AND ADDRESS(ES)

U. S. Army Research Office
P. O. Box 12211
Research Triangle Park, NC 27709-2211

10. SPONSORING/MONITORING AGENCY REPORT NUMBER

ARO 25089.12-EC

11. SUPPLEMENTARY NOTES

The view, opinions and/or findings contained in this report are those of the author(s) and should not be construed as an official Department of the Army position, policy, or decision, unless so designated by other documentation.

12a. DISTRIBUTION/AVAILABILITY STATEMENT

Approved for public release; distribution unlimited.

12b. DISTRIBUTION CODE

13. ABSTRACT (Maximum 200 words)

The purpose of this research project is to study the time domain response of electromagnetic wave radiation, transmission and coupling in multilayered media. The following problems are pursued: (1) extensions and modifications to the double deformation technique; (2) propagation in nonconventional transmission structures; (3) signal distortion at discontinuities; (4) the effects of anisotropic material and nonlinear loads; (5) limitation of quasi-TEM approximation. We shall emphasize and seek to refine a powerful transform-domain formulation, the double deformation technique in order to have a unified way of interpreting the results. Yet other techniques such as the space-time domain integral equation method, the transmission line matrix method, the method of characteristics, and the method of moments are also to be applied to different problems as demanded by efficiency or ease of formulation. The research results can be applied to computer-aided design of hig-speed microelectronic integrated circuits, as well as to time-domain geophysics sub-surface probing, and active remote sensing with transient radar pulses.

14. SUBJECT TERMS			15. NUMBER OF PAGES
			16. PRICE CODE
17. SECURITY CLASSIFICATION OF REPORT	18. SECURITY CLASSIFICATION OF THIS PAGE	19. SECURITY CLASSIFICATION OF ABSTRACT	20. LIMITATION OF ABSTRACT
UNCLASSIFIED	UNCLASSIFIED	UNCLASSIFIED	UL

TIME DOMAIN ELECTROMAGNETIC WAVES IN MULTILAYERED MEDIA

FINAL REPORT

J. A. Kong

Covering 5/1/88-4/30/91

U. S. Army Research Office

Contract number: DAAL03-88-K-0057

Center for Electromagnetic Theory and Applications
Rsearch Laboratory of Electronics
Massachusetts Institute of Technology

FINAL REPORT

Title: TIME DOMAIN ELECTROMAGNETIC WAVES IN MULTILAYERED MEDIA

Sponsor by: Department of the Army
Army Research Office

Contract number: DAAL03-88-K-0057

Research Organization: Center for Electromagnetic Theory and Applications
Research Laboratory of Electronics
Massachusetts Institute of Technology

OSP number: 70458

Principal Investigator: J. A. Kong

Period covered: 1 May 1988 — 30 April 1991

FINAL REPORT

1. ARO PROPOSAL NUMBER: 25089-EL
2. PERIOD COVERED BY REPORT: 1 May 1988 – 30 April 1991
3. TITLE OF PROPOSAL: Time Domain Electromagnetic Waves in Multilayered Media
4. CONTRACT OR GRANT NUMBER: DAAL03-88-K-0057
5. NAME OF INSTITUTION: Massachusetts Institute of Technology
6. AUTHOR OF REPORT: Professor J. A. Kong
7. LIST OF MANUSCRIPTS SUBMITTED OR PUBLISHED UNDER ARO SPONSORSHIP DURING THIS REPORTING PERIOD, INCLUDING JOURNAL REFERENCES:

[1] Propagation properties of strip lines periodically loaded with crossing strips (J. F. Kiang, S. M. Ali, and J. A. Kong), *IEEE Transactions on Microwave Theory and Techniques*, Vol. 37, No. 4, pp. 776 – 786, April 1989.

[2] Transient Analysis of Frequency-Dependent Transmission Line Systems Terminated with Nonlinear Loads (Q. Gu, Y. E. Yang and J. A. Kong), *Journal of Electromagnetic Waves and Application*, Vol.3, No.3, 183–197, 1989.

[3] Integral equation solution to the guidance and leakage properties of coupled dielectric strip waveguides (J. F. Kiang, S. M. Ali, and J. A. Kong), *IEEE Transactions on Microwave Theory and Techniques*, Vol. 38, No. 2, 193 – 203, February 1990.

[4] Input impedance parameters and radiation pattern of cylindrical-rectangular and wraparound microstrip antennas (T. M. Habashy, S. M. Ali, and J. A. Kong), *IEEE Transactions on Antennas and Propagation*, Vol. 38, no. 5 722-731, May 1990.

[5] The propagation characteristics of signal lines with crossing strips in multilayered anisotropic media (C. W. Lam, S. M. Ali, and J. A. Kong), *Journal of Electromagnetic Waves and Applications*, Vol. 4, No. 10, 1005–1021, 1990.

[6] Transient response of sources over layered media using the double deformation method (S. Y. Poh, M. J. Tsuk, and J. A. Kong), *IEEE AP-S International Symposium and URSI Radio Science Meeting*, San Jose, California, June 26-30, 1989.

[7] Resonant frequencies of stacked circular microstrip antennas (A. N. Tulintseff, S. M. Ali, and J. A. Kong), *IEEE AP-S International Symposium and URSI Radio Science Meeting*, San Jose, California, June 26-30, 1989.

[8] Probe excitation of a center-fed circular microstrip antenna employing a stratified medium formulation (S. M. Ali, T. M. Habashy, and J. A. Kong), *IEEE AP-S International Symposium and URSI Radio Science Meeting*, San Jose, California, June 26-30, 1989.

[9] Probe excitation of a center-fed circular microstrip antenna Employing the Weber Transform (T. M. Habashy, S. M. Ali, and J. A. Kong), *IEEE AP-S International Symposium and URSI Radio Science Meeting*, San Jose, California, June 26-30, 1989.

[10] Input impedance and radiation fields of a probe-fed stacked circular microstrip antenna, (A. N. Tulintseff, S. M. Ali, and J. A. Kong), *Progress in Electromagnetics Research Symposium*, Boston, Massachusetts, July 25–26, 1989.

[11] Analysis of microstrip discontinuities on anisotropic substrates, (J. Xia, S.M. Ali, and J. A. Kong), *Progress in Electromagnetics Research Symposium,* Boston, Massachusetts, July 25–26, 1989.

[12] Analysis of dielectric strip waveguides using integral equation formulation, (J. F. Kiang, S. M. Ali, and J. A. Kong), *Progress in Electromagnetics Research Symposium,* Boston, Massachusetts, July 25–26, 1989.

[13] Input impedance of a circular microstrip antenna fed by an eccentric probe, (S.M. Ali, T.M. Habashy, and J.A. Kong), *Progress in Electromagnetics Research Symposium,* Boston, Massachusetts, July 25–26, 1989.

[14] Polarimetric remote sensing of earth terrain with two-layer random medium model, (M. Borgeaud, J.A. Kong, R.T. Shin, and S. V. Nghiem), *Progress in Electromagnetics Research Symposium,* Boston, Massachusetts, July 25–26, 1989.

[15] Finite difference time domain techniques for two dimensional triangular grids, (Check F. Lee, Robert T. Shin, Jin A. Kong, and Brian J. McCartin), *Progress in Electromagnetics Research Symposium,* Boston, Massachusetts, July 25–26, 1989.

[16] Absorbing boundary conditions on circular and elliptic boundaries, (Check F. Lee, Robert T. Shin, Jin A. Kong, and Brian J. McCartin), *Progress in Electromagnetics Research Symposium,* Boston, Massachusetts, July 25–26, 1989.

[17] Far field pattern of a VLF antenna array in the ionospheric plasmas, (H. C. Han and J. A. Kong, and T. M. Habashy), *Progress in Electromagnetics Research Symposium,* Boston, Massachusetts, July 25–26, 1989.

[18] Radar cross section prediction of slots in ground planes using method of moments, (Kevin Li, Robert T. Shin and J. A. Kong), *Progress in Electromagnetics Research Symposium,* Boston, Massachusetts, July 25–26, 1989.

[19] A new finite-difference time-domain grid model for microstrip problems in anisotropic media, (C. W. Lam, S. M. Ali, and J. A. Kong), *Progress in Electromagnetics Research Symposium,* Boston, Massachusetts, July 25–26, 1989.

[20] Faraday polarization fluctuations in transionspheric polarimetric VLF waves, (S. V. Nghiem and J. A. Kong), *Progress in Electromagnetics Research Symposium,* Boston, Massachusetts, July 25–26, 1989.

[21] Analysis of multiport rectangular microstrip structures using a three dimensional finite difference time domain technique, (D. M. Sheen, S. M. Ali, M. D. Abouzahra, and J. A. Kong), *Progress in Electromagnetics Research Symposium,* Boston, Massachusetts, July 25–26, 1989.

[22] The frequency-dependent resistance of conductors with arbitrary cross-section, (M. J. Tsuk and J. A. Kong), *Progress in Electromagnetics Research Symposium,* Boston, Massachusetts, July 25–26, 1989.

[23] Transient analysis of frequency-dependent transmission lines with nonlinear terminations, (Q. Gu, Y. E. Yang and J. A. Kong), *Progress in Electromagnetics Research Symposium,* Boston, Massachusetts, July 25–26, 1989.

[24] Transient analysis of capacitively loaded VLSI off-chip interconnections, (Y. Eric Yang and Jin Au Kong), *Progress in Electromagnetics Research Symposium,* Boston, Massachusetts, July 25–26, 1989.

[25] Input impedance of a circular microstrip antenna fed by an eccentric probe (S. M. Ali, T.

M. Habashy, and J. A. Kong), *Progress in Electromagnetics Research Symposium,* Boston, Massachusetts, July 25-27, 1989.

[26] Integral equation formulation of inhomogeneous slab waveguides (J. F. Kiang, S. M. Ali, and J. A. Kong), *IEEE Journal of Quantum Electronics,* required revision.

[27] Input impedance of a probe-fed stacked circular microstrip antenna (A. N. Tulintseff, S. M. Ali, and J. A. Kong), *IEEE Transactions on Antennas and Propagation,* pp. 381 –390, Vol. 39, No.3, March 1991.

[28] Electro-magnetic calculation of soft X-ray diffraction from nanometer-scale gold structures (M. L. Schattenburg, K. Li, R. T. Shin, J. A. Kong, and H. I. Smith), submitted to The 35th International Symposium on Electron, Ion, and Photon Beams, Seattle, Washington, May 28 – 31, 1991.

[29] Electromagnetic radiation from a VLSI package and heatsink configuration (S. Y. Poh, C. F. Lee, K. Li, R. T. Shin, and J. A. Kong), submitted to *IEEE 1991 International Symposium on Electromagnetic Compatibility,* August 13 – 15, 1991, Hyatt Cherry Hill, Cherry Hill, NJ.

[30] Current distribution, resistance, and inductance for superconducting strip transmission lines (D. M. Sheen, S. M. Ali, D. E. Oates, R. S. Withers, and J. A. Kong), *IEEE Trans. on Applied Superconductivity,* Vol. 1, No. 2, pp. 108–115, June, 1991.

[31] Dyadic Green's functions in a planar stratified, arbitrarily magnetized linear plasma (T. M. Habashy, S. M. Ali, J. A. Kong, and M. D. Grossi), Vol. 26, No. 3, pp. 701–715, May-June, 1991.

[32] Spectral domain dyadic green's function in layered chiral media, (S. M. Ali, T. M. Habashy, J. A. Kong), submitted to *JOSA*, May 1991.

[33] A Hybrid Method for the Calculation of the Resistance and Inductance of Transmission Lines with Arbitrary Cross-Sections (M. J. Tsuk and J. A. Kong), to appear *IEEE Transactions on Microwave Theory and Techniques,* 1991.

[34] Application of the Three Dimensional Finite Difference Time- Domain Method to the Analysis of Planar Microstrip Circuits (D. M. Sheen, S. M. Ali, M. D. Abouzahra, and J. A. Kong), *IEEE Transactions on Microwave Theory and Techniques,* Vol. 38, 849 – 857, July 1990.

[35] Finite Difference Method for Electromagnetic Scattering Problems (C. F. Lee, R. T. Shin, and J. A. Kong), *Progress In Electromagnetics Research,* Vol. 4, Ch. 11, 373-442, Elsevier, New York, 1990.

[36] Absorbing Boundary Conditions on Circular and Elliptic Boundaries (C. F. Lee, R. T. Shin, J. A. Kong, and B. J. McCartin), *Journal of Electromagnetic Waves and Applications,* Vol. 4, No. 10, 945–962, 1990.

[37] Modelling of Lossy Microstrip Lines with Finite Thickness (J. F. Kiang, S. M. Ali, and J. A. Kong), *Progress In Electromagnetics Research*, Vol. 4, Ch. 3, 85–117, Elsevier, New York, 1990.

[38] Inversion of Permittivity and Conductivity Profiles Employing Transverse-Magnetic Polarized Monochromatic Data (T. M. Habashy, M. Moldoveanu, and J. A. Kong), *SPIE's 1990 International Symposium on Optical and Optoelectronic Applied Science and Engineering*, San Diego, California, July 8 – 13, 1990.

[39] Analysis of Diffraction from Chiral Gratings (S. H. Yueh and J. A. Kong), accepted for publication in *Journal of Electromagnetic Waves and Applications.,* 1990.

[40] A Theoretical Analysis of a Probe-Fed Stacked Circular Microstrip Antenna (A. N. Tulintseff), Ph.D. dissertation, Department of Electrical Engineering and Computer Science, M.I.T., September 1990.

[41] Variance of Phase Fluctuations of Waves Propagating Through a Random Medium (N. C. Chu, J. A. Kong, H. A. Yueh, S. V. Nghiem, J. G. Fleischman, S. Ayasli, and R. T. Shin), accepted for publication in *Journal of Electromagnetic Waves and Applications*, 1990.

8. SCIENTIFIC PERSONNEL SUPPORTED BY THIS PROJECT AND DEGREES AWARDED DURING THIS REPORTING PERIOD:

Jin Au Kong:	Principal Investigator
Sami M. Ali:	Research Scientist
Michael J. Tsuk:	Graduate Student-Ph.D 1990
Ann N. Tulintseff:	Graduate Student-Ph.D 1990
Son V. Nghiem:	Graduate Student-Ph.D 1991
Simon H. Yueh:	Graduate Student-Ph.D 1991
David M. Sheen:	Graduate Student-Ph.D 1991
Eric Y. Yang:	Graduate Student-Ph.D 1989 Research Scientist
Cheung W. Lam:	Graduate Student-M.S.-1989

Jin-Au Kong
Department of Electrical Engineering
and Computer Science
MIT, Room 26-305
Cambridge, MA 02139

STATEMENT OF WORK

The purpose of this research project is to study the time domain response of electromagnetic wave radiation, transmission, and coupling in multilayered media. The following problems are pursued: (1) extensions and modifications to the double deformation technique; (2) propagation in nonconventional transmission structures; (3) signal distortion at discontinuities; (4) the effects of anisotropic material and nonlinear loads; (5) limitation of quasi-TEM approximation. We shall emphasize and seek to refine a powerful transform-domain formulation, the double deformation technique in order to have a unified way of interpreting the results. Yet other techniques such as the space-time domain integral equation method, the transmission line matrix method, the method of characteristics, and the method of moments are also to be applied to different problems as demanded by efficiency or ease of formulation. The research results can be applied to computer-aided design of high-speed microelectronic integrated circuits, as well as to time-domain geophysics subsurface probing, and active remote sensing with transient radar pulses.

SUMMARY OF RESEARCH FINDINGS

The guidance and leakage properties of single and coupled dielectric strip waveguides are analyzed using the dyadic Green's function and integral equation formulation. Galerkin's method is used to solve the integral equation for the dispersion relation. The effects of the geometrical and the electrical parameters on the dispersion relation are investigated. A method to predict the occurrence of leakage is proposed. The properties of the even and the odd leaky modes are also investigated. Results are compared with previous analysis and shown to be in good agreement.

The input impedance of a microstrip antenna consisting of two circular microstrip disks in a stacked configuration driven by a coaxial probe is investigated. A rigorous analysis is performed using a dyadic Green's function formulation where the mixed boundary value problem is reduced to a set of coupled vector integral equations using the vector Hankel transform. Galerkin's method is employed in the spectral domain where two sets of disk current expansions are used. One set is based on the complete set of orthogonal modes of the magnetic cavity, and the other employs Chebyshev polynomials with the proper edge condition for the disk currents. An additional term is added to the disk current expansion to properly model the current in the vicinity of the probe/disk junction. The input impedance of the stacked microstrip antenna including the probe self-impedance is calculated as a function of the layered parameters and the ratio of the two disk radii. Disk current distributions and radiation patterns are also presented. The calculate results are compared with experimental data and shown to be in good agreement.

The frequency-dependent resistance and inductance of uniform transmission lines are calculated with a hybrid technique, which is a combination of a cross-section coupled circuit method and a surface integral equation approach. The coupled circuit approach is most applicable for low-frequency calculations, while the integral equation approach is best for high frequencies. The low-frequency method consists of subdividing the cross-section of each conductor into triangular filaments, each with an assumed uniform current distribution. The resistance and mutual inductance between the filaments are calculated, and a matrix is inverted to give the overall resistance and inductance of the conductors. The high-frequency method expresses the resistance and inductance of each conductor in terms of the current at the surface of that conductor and the derivative of that current normal to the surface. A coupled integral equation is then derived to relate these quantities through the diffusion equation inside the conductors and Laplace's equation outside. The method of moments with pulse basis functions is used to solve the integral equations. An

interpolation between the results of these two methods gives very good results over the entire frequency range, even when few basis functions are used.

Because the effects of diffraction during proximity-print x-ray lithography are of critical importance, a number of previous researchers have attempted to calculate the diffraction patterns and minimum achievable feature sizes as a function of wavelength and gap. Work to date has assumed that scalar diffraction theory is applicable–as calculated, for example, by the Rayleigh-Sommerfeld formulation–and that Kirchhoff boundary conditions can be applied. Kirchhoff boundary conditions assume that the fields (amplitude and phase) are constant in the open regions between absorbers, and a different constant in regions just under the absorbers (i.e., that there are no fringing fields). An x-ray absorber is, however, best described as a lossy dielectric that is tens or hundreds of wavelengths tall, and hence Kirchhoff boundary conditions are unsuitable. We found out that the use of Kirchhoff boundary conditions introduces unphysically high spatial frequencies into the diffracted fields. The suppression of these frequencies–which occurs naturally without the need to introduce an extended source or broad spectrum–improves exposure latitude for mask features near 0.1 μm and below.

The electromagnetic radiation from a VLSI chip package and heatsink structure is analysed by means of the finite-difference time-domain (FD-TD) method. The FD-TD algorithm implemented incorporates a multi-zone gridding scheme to accommodate fine grid cells in the vicinity of the heatsink and package cavity and sparse gridding in the remainder of the computational domain. The issues pertaining to the effects of the heatsink in influencing the overall radiating capacity of the configuration are addressed. Analyses are facilitated by using simplified heatsink models and by using dipole elements as sources of electromagnetic energy to model the VLSI chip. The potential for enhancement of spurious emissions by the heatsink structure is illustrated. For heatsinks of typical dimensions, resonance is possible within the low gigahertz frequency range. The potential exploitation of the heatsink as an emissions shield by appropriate implementation schemes is discussed and evaluated.

A method for the calculation of the current distribution, resistance, and inductance matrices for a system of coupled superconducting transmission lines having finite rectangular cross section is derived. These calculations allow accurate characterization of both high-T_c and low-T_c superconducting strip transmission lines. For a single stripline geometry with finite ground planes, the current distribution, resistance, inductance, and kinetic inductance are calculated as a function of the penetration depth for various film thickness. These calculations are then used to determine the penetration depth for Nb, NbN, and $YBa_2Cu_3O_{7-x}$ superconducting thin films from the measured temperature dependence of the resonant frequency of a stripline resonator. The calculations are also used to convert measured temperature dependence of the quality factor to the intrinsic surface resistance as a function of temperature for a Nb stripline resonator.

A general spectral domain formulation to the problem of radiation of arbitrary distribution of sources embedded in a horizontally stratified arbitrary magnetized linear plasma is presented. The fields are obtained in terms of electric and magnetic type dyadic Green's functions. The formulation is considerably simplified by using the kDB system of coordinates in conjunction with the Fourier transform. The distributional singular behavior of the various dyadic Green's functions in the source region is investigated and taken into account by extracting the delta function singularities. Finally, the fields in any arbitrary layer are obtained in terms of appropriately defined global upward and downward reflection and transmission matrices.

A spectral domain dyadic Green's function formulation defining the fields inside a multilayer chiral medium due to arbitrary distribution of sources is presented. The constitutive parameters and the chirality of each layer are assumed to be different. The fields are obtained in terms of electric and magnetic type dyadic Green's functions. The singular behavior of these dyadic Green's functions in the source region is taken into account by extracting the delta function singularities. The fields in any layer are obtained in terms of appropriately defined global reflection and transmission matrices.

The frequency-dependent resistance and inductance of uniform transmission lines are calculated using a hybrid technique, which is a combination of a cross-section finite element method and a surface integral equation approach. The finite element approach is most applicable for low-frequency calculations, while the integral equation approach is best for high frequencies. An interpolation between the results of these two methods gives very good results over the entire frequency range, even when few basis functions are used. Using this method, a potential CAD tool for the calculation of transmission line parameters is developed.

A direct three-dimensional finite-difference time-domain (FDTD) method is applied to the full-wave analysis of various microstrip structures. The method is shown to be an efficient tool for modeling complicated microstrip circuit components as well as microstrip antennas. From the time-domain results, the input impedance of a line-fed rectangular patch antenna and the frequency-dependent scattering parameters of a low-pass filter and a branch line coupler are calculated. These circuits are fabricated and the measurements are compared with the FDTD results and shown to be in good agreement. A general purpose time-domain numerical algorithm for modelling three-dimensional microstrip structures is developed.

The pseudo-differential operator approach is employed to derive absorbing boundary conditions for both circular and elliptical outer boundaries. The pseudo-differential operator approach employed by Engquist and Majda is modified to derive improved absorbing boundary conditions. In the case of circular outer boundaries, the modified pseudo-differential operator approach leads to a condition equivalent to that of Bayliss and Turkel's

second-order condition. The modified pseudo-differential operator is then used to derive the second-order absorbing boundary condition for elliptical outer boundaries. The effectiveness of the second-order absorbing boundary condition on elliptical outer boundary is illustrated by calculating scattered fields from various objects. It is shown that for elongated scatterers, the elliptical outer boundary can be used to reduce the size of the computational domain.

Quasi-TEM approximation is applied to the analysis of coupled lossy microstrip lines with finite thickness embedded in a horizontally stratified medium. A scalar Green's function in the spectral domain is used to obtain a set of coupled integral equations for the surface charge distribution. The method of moments is then used to find the charge distribution and hence the capacitance matrix of the microstrip lines. The inductance and the conductance matrices are obtained by using the duality between the magnetostatic problem, the current field problem, and the electrostatic problem. The resistance matrix is obtained by a perturbation method. A multiconductor transmission line analysis is derived by using the capacitance, the inductance, the conductance, and the resistance matrices. The transient response is obtained by using the Fourier transform.

An inversion algorithm based on a recently developed inversion method referred to as the Renormalized Source-Type Integral Equation approach is developed. The objective of this method is to overcome some of the limitations and difficulties of the iterative Born technique. It recasts the inversion, which is nonlinear in nature, in terms of the solution of a set of linear equations; however, the final inversion equation is still nonlinear. The derived inversion equation is an exact equation which sums up the iterative Neuman (or Born) series in a closed form and; thus, is a valid representation even in the case when the Born series diverges.

The coupled-wave theory is generalized to analyze the diffraction of waves by chiral gratings for arbitrary angle of incidence and polarizations. Numerical results are obtained for the Stokes parameters of diffracted Floquet modes versus the thickness of chiral gratings with various chiralities. Both horizontal and vertical incidences are considered. The diffracted waves from chiral gratings are in general elliptically polarized; and at some particular instances, it is possible for chiral gratings to convert a linearly polarized incident field into two nearly circularly polarized Floquet modes propagating in different directions.

A theoretical analysis of a circular microstrip antenna consisting of two disks in a stacked configuration driven by a coaxial probe is presented. The resonant frequencies, input impedance, radiation fields, and receiving and scattering characteristics are investigated. For each of the problems presented, a rigorous analysis is performed using a dyadic Green's function formulation. Employing the vector Hankel transform, the problem is reduced to a set of coupled vector integral equations and solved using Galerkin's method in the spectral domain. The scattering, receiving, and transmitting characteristics

of an infinite array of probe-fed stacked circular microstrip antennas are also investigated. The input impedance, scanning performance, and cross polarization levels are thoroughly investigated.

Proposal Number 25089-EL
Funding Document DAAL03-88-K-0057

We have not received the reprints of the following manuscripts yet:

"Resonant Frequencies of Stacked Circular Microstrip Antennas," by A. N. Tulintseff et al.

"Input Impedance and Radiation Pattern of Cylindrical-Rectangular and Wrap-around Microstrip Antennas," by T. M. Habashy et al.

"Finite-Difference Time-Domain Method for Single and Coupled Microstrip Lines," by C. W. Lam et al.

Input Impedance of a Probe-Fed Stacked Circular Microstrip Antenna

Ann N. Tulintseff, Sami M. Ali, *Senior Member, IEEE*, and Jin Au Kong, *Fellow, IEEE*

Abstract—**The input impedance of a microstrip antenna consisting of two circular microstrip disks in a stacked configuration driven by a coaxial probe is investigated. A rigorous analysis is performed using a dyadic Green's function formulation where the mixed boundary value problem is reduced to a set of coupled vector integral equations using the vector Hankel transform. Galerkin's method is employed in the spectral domain where two sets of disk current expansions are used. One set is based on the complete set of orthogonal modes of the magnetic cavity, and the other employs Chebyshev polynomials with the proper edge condition for the disk currents. An additional term is added to the disk current expansion to properly model the current in the vicinity of the probe/disk junction. The input impedance of the stacked microstrip antenna including the probe self-impedance is calculated as a function of the layered parameters and the ratio of the two disk radii. Disk current distributions and radiation patterns are also presented. The calculated results are compared with experimental data and shown to be in good agreement.**

I. Introduction

CONVENTIONAL microstrip antennas, consisting of a single conducting patch on a grounded dielectric substrate, have received much attention in recent years [1] due to their many advantages, including low profile, light weight, and easy integration with printed circuits. However, due to their resonant behavior, they radiate efficiently only over a narrow band of frequencies, with bandwidths typically only a few percent [1]. While maintaining the advantages of conventional single patch microstrip antennas, microstrip antennas of stacked configurations, consisting of one or more conducting patches parasitically coupled to a driven patch, overcome the inherent narrow bandwidth limitation by introducing additional resonances in the frequency range of operation, achieving bandwidths up to 10–20%. In addition, stacked microstrip configurations have achieved higher gains and offer the possibility of dual frequency operation.

Experimental work with multilayered microstrip elements has been abundant [2]–[9]. However, to date, theoretical work has been relatively limited, where the study of resonant frequencies, modes and radiation patterns have been investigated [10]–[13]. Recently, the finite-difference time-domain technique was applied to stacked rectangular microstrip patch configurations [14]. There is little or no theoretical analysis of the input impedance of coaxial probe-fed stacked circular microstrip patches. However, the input impedance for conventional single-layer coaxial probe-fed microstrip antennas of circular, rectangular, annular ring, and elliptic geometries has been investigated by many authors [15]–[19]. The impedance parameters of two planar coupled microstrip patches have also been studied [19], [20].

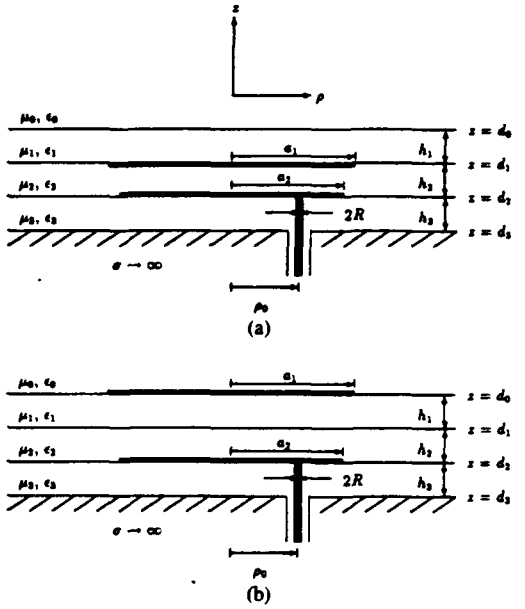

Fig. 1. Stacked microstrip antenna configurations.

In the calculation of the input impedance of probe-driven microstrip antennas on thin substrates, the effect of the probe results in an additional inductive component to the input impedance. This probe inductance has been accounted for by several authors through use of a simple formula [19], [21]. In more rigorous methods to include the effects of the probe, an "attachment mode" in the disk current expansion is used to account for the singular behavior of the disk current in the vicinity of the probe, ensure continuity of the current at the probe/disk junction, and speed up the convergence of the solution. An "attachment mode" which represented the disk current of a lossy magnetic cavity driven by a uniform cylindrical probe current was introduced in [16]. More recently, similar and other "attachment modes," with the $1/\rho$ dependence in the vicinity of the probe and the appropriate boundary condition on normal current, defined over the entire disk or locally over a portion of the disk, have also been used [22]–[25]. In a different approach, the effects of the probe were accounted for by expanding the currents on the disk and probe in terms of the modes of a cylindrical magnetic cavity satisfying boundary conditions on the eccentrically located probe [26].

Considered here is a microstrip antenna consisting of two circular microstrip disks in a stacked configuration driven by a coaxial probe. The two stacked configurations shown in Figs. 1(a) and 1(b), denoted configurations A and B, respectively, are investigated. The disks are assumed to be infinitesimally thin and

Manuscript received March 12, 1990; revised July 27, 1990. This work was supported by RADC under Contract F19628-88-K-0013, the ARO under Contract DAAL03-88-K-0057, the ONR under Contract N00014-90-J-1002, the Joint Services Electronics Program under Contract DAAL03-89-C-0001, and NSF Grant ECS86-20029.

The authors are with the Department of Electrical Engineering and Computer Science and Research Laboratory of Electronics, Massachusetts Institute of Technology, Cambridge, MA 02139.

IEEE Log Number 9041263.

perfectly conducting and the substrates are taken to be infinite in extent. A rigorous analysis of the two stacked circular disks in a layered medium is performed using a dyadic Green's function formulation. Using the vector Hankel transform, the mixed boundary value problem is reduced to a set of coupled vector integral equations and solved by employing Galerkin's method in the spectral domain. Two solutions using two different basis sets to expand the unknown disk currents are developed. The first set of basis functions used are the complete set of transverse magnetic (TM) and transverse electric (TE) modes of a cylindrical cavity with magnetic side walls. The second set of basis functions used employ Chebyshev polynomials and enforce the current edge condition. An additional term in the current expansion is taken to account for the singular nature of the current on the disk in the vicinity of the probe and to ensure continuity of current at the junction. This term, the "attachment mode," is taken to be the disk current of a magnetic cavity under a uniform cylindrical current excitation. It is shown here explicitly that continuity of the current at the probe/disk junction must be enforced to rigorously include the probe self-impedance. The convergence of the results is investigated and ensured by using a proper number of basis functions. The input impedance of the stacked microstrip antenna is calculated for different configurations of substrate parameters and disk radii. Disk current distributions and radiation patterns are also presented. Finally, the results are compared with experimental data and shown to be in good agreement. Throughout the analysis, the $\exp(-i\omega t)$ time dependence is used and suppressed.

II. Dyadic Green's Function and Integral Equation Formulation

For a general formulation which applies to both configurations A and B of Fig. 1, we consider two coaxial, circular perfectly conducting disks, of radii a_1 and a_2, carrying current distributions $\bar{J}_j(\bar{r}) = \bar{K}_j(\bar{\rho})\delta(z - z_j')$ where $j = (1, 2)$ and $\delta(\cdot)$ is the Dirac delta function. Configuration A is obtained when $z_1' = d_1$ and $z_2' = d_2$ and configuration B results when $z_1' = d_0$ and $z_2' = d_2$.

Using the induced EMF method [27], a stationary formula for the input impedance is obtained as

$$Z_{in} = -\frac{1}{I^2}\iiint dV\,\bar{E}(\bar{r})\cdot\bar{J}_{probe}(\bar{r}) \tag{1}$$

where $\bar{J}_{probe}$ is the current distribution on the probe and $\bar{E}$ is the total electric field due to the probe current and induced disk currents.

The current on the probe, of radius R and at the position $\bar{\rho}_0 = (\rho_0, \phi_0)$, is taken to be uniform and is given by

$$\bar{J}_{probe}(\bar{\rho}, z) = \hat{z}\frac{I}{2\pi R}\delta(\rho_p - R), \qquad d_2 < z < d_2 \tag{2}$$

with local coordinates defined as $\bar{\rho}_p = \bar{\rho} - \bar{\rho}_0 = (\rho_p, \phi_p)$.

Using a dyadic Green's function formulation in cylindrical coordinates for horizontally stratified media [11], we obtain expressions for the transverse components of the electric fields due to the disk and probe current distributions. Boundary conditions require that the transverse components of the electric field vanish on the perfectly conducting disks and the currents vanish off the disks, to give the following set of coupled integral equations for the disk currents

$$\begin{aligned}\left[\bar{E}(\bar{\rho}, z = z_j')\right]_T = &\sum_{m=-\infty}^{\infty} e^{im\phi}\int_0^{\infty} dk_\rho\, k_\rho \bar{\bar{J}}_m(k_\rho\rho)\\ &\cdot \bar{\bar{\xi}}_{j,1}(k_\rho, z = z_j', z' = z_1')\cdot\bar{\kappa}_m^{(1)}(k_\rho)\\ &+\sum_{m=-\infty}^{\infty} e^{im\phi}\int_0^{\infty} dk_\rho\, k_\rho \bar{\bar{J}}_m(k_\rho\rho)\\ &\cdot \bar{\bar{\xi}}_{j,2}(k_\rho, z = z_j', z' = z_2')\cdot\bar{\kappa}_m^{(2)}(k_\rho)\\ &+\sum_{m=-\infty}^{\infty} e^{im\phi}\int_0^{\infty} dk_\rho\, k_\rho \bar{\bar{J}}_m(k_\rho\rho)\\ &\cdot \bar{\bar{\xi}}_{j,3}^{TM}(k_\rho, z = z_j')\cdot\bar{p}_m(k_\rho)\\ = 0, &\qquad \rho < a_j\end{aligned} \tag{3}$$

$$\begin{aligned}\bar{K}_m^{(j)}(\rho) = &\int_0^{\infty} d\rho\,\rho\,\bar{\bar{J}}_m(k_\rho\rho)\\ &\cdot\bar{\kappa}_m^{(j)}(k_\rho) = 0, \qquad \rho > a_j\end{aligned} \tag{4}$$

where $j = 1, 2$, and k_ρ is the transverse wavenumber satisfying the dispersion relation

$$k_\rho^2 + k_{lz}^2 = k_l^2 = \omega^2\mu_l\epsilon_l \tag{5}$$

in each region l. In (3), z and z' correspond to the longitudinal positions of observer and source, respectively. $\bar{\kappa}_m^{(1)}(k_\rho)$ and $\bar{\kappa}_m^{(2)}(k_\rho)$ are the vector Hankel transforms of the two disk currents $\bar{K}_m^{(1)}(\rho)$ and $\bar{K}_m^{(2)}(\rho)$, respectively, defined by

$$\bar{\kappa}_m^{(j)}(k_\rho) = \int_0^{\infty} d\rho\,\rho\,\bar{\bar{J}}_m^{\dagger}(k_\rho\rho)\cdot\bar{K}_m^{(j)}(\rho) \tag{6}$$

where $\bar{K}_m^{(j)}(\rho)$ is the Fourier coefficient

$$\bar{K}_m^{(j)}(\rho) = \frac{1}{2\pi}\int_0^{2\pi} d\phi\, e^{-im\phi}\bar{K}_j(\bar{\rho}) \tag{7}$$

and $\bar{\bar{J}}_m(k_\rho\rho)$ is the kernel of the vector Hankel transform (VHT) [28] given by

$$\bar{\bar{J}}_m(k\rho\rho) = \begin{bmatrix} J_m'(k_\rho\rho) & \dfrac{-im}{k_\rho\rho}J_m(k_\rho\rho)\\ \dfrac{im}{k_\rho\rho}J_m(k_\rho\rho) & J_m'(k_\rho\rho)\end{bmatrix}. \tag{8}$$

$J_m(\cdot)$ is the Bessel function of the first kind of order m and the prime denotes differentiation with respect to the argument. $\bar{\bar{J}}_m^{\dagger}(k_\rho\rho)$ is the complex conjugate transpose of $\bar{\bar{J}}_m(k_\rho\rho)$.

In the last term of (3), $\bar{p}_m(k_\rho)$ is associated with the probe current and is given by

$$\bar{p}_m(k_\rho) = \begin{bmatrix} p_m(k_\rho)\\ 0\end{bmatrix} \tag{9}$$

where

$$p_m(k_\rho) = -\frac{I}{2\pi}\frac{k_\rho}{k_{3z}^2}J_m(k_\rho\rho_0)\,J_0(k_\rho R)e^{-im\phi_0}. \tag{10}$$

The matrix $\bar{\bar{\xi}}_{l,3}^{TM}(k_\rho, z)$ includes the effects of the stratified medium when relating the probe current to the transverse elec-

tric fields and is defined as

$$\bar{\bar{\xi}}_{l,3}^{\mathrm{TM}}(k_\rho, z) = \begin{bmatrix} \xi_{l,3}^{\mathrm{TM}} & 0 \\ 0 & 0 \end{bmatrix}. \tag{11}$$

It is clear that the assumed probe current excites TM modes only. The matrices $\bar{\bar{\xi}}_{l,j}(k_\rho, z, z')$ with $l, j = (1,2)$ in (3) include the effects of the stratified medium when relating the disk currents to transverse electric fields and are of the form

$$\bar{\bar{\xi}}_{l,j}(k_\rho, z, z') = \begin{bmatrix} \xi_{l,j}^{\mathrm{TM}} & 0 \\ 0 & \xi_{l,j}^{\mathrm{TE}} \end{bmatrix}. \tag{12}$$

The expressions for $\xi_{l,3}^{\mathrm{TM}}(k_\rho, z)$, $\xi_{l,j}^{\mathrm{TM}}(k_\rho, z, z')$, and $\xi_{l,j}^{\mathrm{TE}}(k_\rho, z, z')$ are given in the Appendix.

III. Galerkin's Method

Galerkin's method is employed to solve the coupled vector integral equations of (3) and (4). The currents on the circular disks are expanded in terms of a set of basis functions

$$\bar{K}_m^{(1)}(\rho) = \sum_n^N a_{mn}^{(1)} \bar{\Psi}_{mn}^{(1)}(\rho) + \sum_p^P b_{mp}^{(1)} \bar{\Phi}_{mp}^{(1)}(\rho) \tag{13a}$$

$$\bar{K}_m^{(2)}(\rho) = \sum_r^R a_{mr}^{(2)} \bar{\Psi}_{mr}^{(2)}(\rho) + \sum_s^S b_{ms}^{(2)} \bar{\Phi}_{ms}^{(2)}(\rho) + \bar{K}_{m,att}^{(2)}(\rho). \tag{13b}$$

N and P correspond to the number basis functions $\bar{\psi}_{mj}(\rho)$ and $\bar{\phi}_{mj}(\rho)$, respectively, taken for the upper disk and R and S correspond to those taken for the lower disk. $\bar{K}_{m,att}^{(2)}(\rho)$ is the "attachment mode."

The corresponding VHT of the currents is given by

$$\bar{\kappa}_m^{(1)}(k_\rho) = \sum_n^N a_{mn}^{(1)} \bar{\psi}_{mn}^{(1)}(k_\rho) + \sum_p^P b_{mp}^{(1)} \bar{\phi}_{mp}^{(1)}(k_\rho) \tag{14a}$$

$$\bar{\kappa}_m^{(2)}(k_\rho) = \sum_r^R a_{mr}^{(2)} \bar{\psi}_{mr}^{(2)}(k_\rho) + \sum_s^S b_{ms}^{(2)} \bar{\phi}_{ms}^{(2)}(k_\rho) + \bar{\kappa}_{m,att}^{(2)}(k_\rho). \tag{14b}$$

A. TM and TE Modes of Cylindrical Cavities with Magnetic Side Walls

One set of basis functions taken are those currents associated with the complete orthogonal set of TM and TE modes of a cylindrical cavity of radius a_j $(j = 1, 2)$ with magnetic side walls and electric top and bottom walls. These current modes are given by

$$\bar{\Psi}_{mn}^{(j)}(\rho) = \begin{cases} \begin{bmatrix} J_m'(\beta_{mn}\rho/a_j) \\ \dfrac{ima_j}{\beta_{mn}\rho} J_m(\beta_{mn}\rho/a_j) \end{bmatrix}, & \text{for } \rho < a_j \\ 0, & \text{for } \rho > a_j \end{cases} \tag{15a}$$

$$\bar{\Phi}_{mp}^{(j)}(\rho) = \begin{cases} \begin{bmatrix} \dfrac{-ima_j}{\alpha_{mp}\rho} J_m(\alpha_{mp}\rho/a_j) \\ J_m'(\alpha_{mp}\rho/a_j) \end{bmatrix}, & \text{for } \rho < a_j \\ 0, & \text{for } \rho > a_j \end{cases} \tag{15b}$$

for $m = 0, \pm 1, \pm 2, \cdots$, $n = 1, 2, \cdots$, and $p = 1, 2, \cdots$ $\bar{\Psi}_{mn}^{(j)}(\rho)$ correspond to the TM cavity modes and $\bar{\Phi}_{mn}^{(j)}(\rho)$ correspond to the TE cavity modes. The constants β_{mn} and α_{mp} correspond to the nth and pth zeros of $J_m'(\beta_{mn}) = 0$ and $J_m(\alpha_{mp}) = 0$, respectively. The VHT of these basis functions is

$$\bar{\psi}_{mn}^{(j)}(k_\rho) = \beta_{mn} J_m(\beta_{mn}) \begin{bmatrix} \dfrac{J_m'(k_\rho a_j)}{(\beta_{mn}/a_j)^2 - k_\rho^2} \\ \dfrac{ima_j}{\beta_{mn}^2 k_\rho} J_m(k_\rho a_j) \end{bmatrix} \tag{16a}$$

$$\bar{\phi}_{mp}^{(j)}(k_\rho) = \frac{k_\rho a_j J_m'(\alpha_{mp})}{k_\rho^2 - (\alpha_{mp}/a_j)^2} \begin{bmatrix} 0 \\ J_m(k_\rho a_j) \end{bmatrix}. \tag{16b}$$

B. Chebyshev Polynomial Expansion with Edge Condition

The second set of basis functions taken includes the edge condition for the disk currents and is taken to be [23]

$$\bar{\Psi}_{mn}^{(j)}(\rho) = \begin{cases} \hat{\rho} T_n(\rho/a_j) \sqrt{1 - \rho^2/a_j^2}, & \text{for } \rho < a_j \\ 0, & \text{for } \rho > a_j \end{cases} \tag{17a}$$

$$\bar{\Phi}_{mn}^{(j)}(\rho) = \begin{cases} \hat{\phi} T_n(\rho/a_j) / \sqrt{1 - \rho^2/a_j^2}, & \text{for } \rho < a_j \\ 0, & \text{for } \rho > a_j \end{cases} \tag{17b}$$

for $m = 0, \pm 1, \pm 2, \cdots$ and $n = 0, 1, 2, \cdots$ $T_n(x)$ is the Chebyshev polynomial [29] and satisfies the recursion formula $T_{n+1}(x) - 2xT_n(x) + T_{n-1}(x) = 0$ with $T_0(x) = 1$ and $T_1(x) = x$. The term $\sqrt{1 - \rho^2/a_j^2}$ provides for the proper singular edge behavior for the azimuthally directed current and the zero edge condition for the normally directed current. Since the current basis functions must have continuous current distributions on the disk, the mode index m and the Chebyshev polynomial index n may not be both even or both odd when performing the current expansion.

The VHT of the above basis functions is given by

$$\bar{\psi}_{mn}^{(j)}(k_\rho) = \begin{bmatrix} I_{mn}^{\psi(j)}(k_\rho) - mJ_{mn}^{\psi(j)}(k_\rho) \\ imJ_{mn}^{\psi(j)}(k_\rho) \end{bmatrix} \tag{18a}$$

$$\bar{\phi}_{mn}^{(j)}(k_\rho) = \begin{bmatrix} -imJ_{mn}^{\phi(j)}(k_\rho) \\ I_{mn}^{\phi(j)}(k_\rho) - mJ_{mn}^{\phi(j)}(k_\rho) \end{bmatrix} \tag{18b}$$

for $m \geq 0$. The integrals, with $y_j = k_\rho a_j$, are defined by

$$\begin{aligned} I_{mn}^{\psi(j)} = \frac{a_j^2}{8} \frac{4}{y_j} \frac{\pi}{2} \Bigg[& -\left(\frac{m-n-2}{2}\right) \\ & \cdot J_{(m+n+2)/2}(y_j/2) J_{(m-n-2)/2}(y_j/2) \\ & -\left(\frac{m+n-2}{2}\right) J_{(m+n-2)/2}(y_j/2) \\ & \cdot J_{(m-n+2)/2}(y_j/2) \\ & + mJ_{(m+n)/2}(y_j/2) J_{(m-n)/2}(y_j/2) \Bigg] \end{aligned} \tag{19a}$$

$$I_{mn}^{\psi(J)} = \frac{a_j^2}{4}\frac{1}{y_j}\frac{\pi}{2}\left[-J_{(m+n+2)/2}(y_j/2)\,J_{(m-n-2)/2}(y_j/2) + 2\,J_{(m+n)/2}(y_j/2)\,J_{(m-n)/2}(y_j/2) - J_{(m+n-2)/2}(y_j/2)\,J_{(m-n+2)/2}(y_j/2)\right] \quad (19b)$$

$$I_{mn}^{\phi(J)} = \frac{a_j^2}{2}\frac{\pi}{2}\left[J_{(m+n)/2}(y_j/2)\,J_{(m-n-2)/2}(y_j/2) + J_{(m+n-2)/2}(y_j/2)\,J_{(m-n)/2}(y_j/2)\right] \quad (19c)$$

$$I_{mn}^{\phi(J)} = \frac{a_j^2}{y_j}\frac{\pi}{2}\left[J_{(m+n)/2}(y_j/2)\,J_{(m-n)/2}(y_j/2)\right]. \quad (19d)$$

In the above expressions, when m and n are not both even or both odd, the Bessel functions $J_{M/2}(\cdot)$ are of half-integer order [30].

C. Attachment Mode

The "attachment mode" term in the current expansion is taken to approximate the rapidly varying currents in the vicinity of the probe/disk junction, ensure continuity of the current, and speed up the convergence of the solution. This term is taken as the disk current of a magnetic cavity of radius a_2 due to a uniform cylindrical current source of radius R positioned at $\bar{\rho}_0$ and given by

$$\bar{K}_{att}^{(2)}(\bar{\rho}) = \frac{I}{2\pi}\sum_{m=-\infty}^{\infty} e^{im(\phi-\phi_0)}\int_0^{\infty} dk_\rho \frac{k_\rho^2}{k_{3z}^2} \cdot J_0(k_\rho R)\,J_m(k_\rho\rho_0)\begin{bmatrix} J_m'(k_\rho\rho) \\ \dfrac{im}{k_\rho\rho}J_m(k_\rho\rho)\end{bmatrix} + \frac{ik_3 I}{4}\sum_{m=-\infty}^{\infty} e^{im(\phi-\phi_0)} \cdot \frac{J_0(k_3R)\,J_m(k_3\rho_0)\,H_m^{(1)\prime}(k_3a_2)}{J_m'(k_3a_2)} \cdot \begin{bmatrix} J_m'(k_3\rho) \\ \dfrac{im}{k_3\rho}J_m(k_3\rho)\end{bmatrix}, \quad 0 \le \rho \le a_2 \quad (20)$$

where $H_m^{(1)}(\cdot)$ is the Hankel function of the first kind of order m. The first term in (20) is the current induced on infinite parallel conducting planes by a uniform cylindrical current. The second term is a homogeneous solution to the wave equation added to satisfy the boundary condition $\bar{H}_{tan}(\rho = a_2) = 0$, providing for vanished normal current at the edge of the disk.

The VHT of the above attachment mode current distribution has a closed form analytic expression given by

$$\bar{\kappa}_{m,att}^{(2)}(k_\rho) = \frac{I}{2\pi}e^{-im\phi_0}\frac{k_\rho}{k_{3z}^2}J_0(k_\rho R)\,J_m(k_\rho\rho_0)\begin{bmatrix}1\\0\end{bmatrix} - \frac{I}{2\pi}e^{-im\phi_0}\frac{J_0(k_3R)\,J_m(k_3\rho_0)}{J_m'(k_3a_2)} \cdot \begin{bmatrix} \dfrac{k_3}{k_{3z}^2}J_m'(k_\rho a_2) \\ \dfrac{im}{k_3a_2k_\rho}J_m(k_\rho a_2)\end{bmatrix}. \quad (21)$$

D. Matrix Equation

Substituting the current expansion of (14) into (3), and applying Parseval's theorem, we obtain a system of $N + P + R + S$ linear algebraic equations for each mode m which may be written in matrix form

$$\bar{\bar{A}}_m \cdot \bar{c}_m = \bar{d}_m \quad (22)$$

where

$$\bar{\bar{A}}_m = \begin{bmatrix} [A]_{N\times N}^{\psi(1)\psi(1)} & [A]_{N\times P}^{\psi(1)\phi(1)} & [A]_{N\times R}^{\psi(1)\psi(2)} & [A]_{N\times S}^{\psi(1)\phi(2)} \\ [A]_{P\times N}^{\phi(1)\psi(1)} & [A]_{P\times P}^{\phi(1)\phi(1)} & [A]_{P\times R}^{\phi(1)\psi(2)} & [A]_{P\times S}^{\phi(1)\phi(2)} \\ [A]_{R\times N}^{\psi(2)\psi(1)} & [A]_{R\times P}^{\psi(2)\phi(1)} & [A]_{R\times R}^{\psi(2)\psi(2)} & [A]_{R\times S}^{\psi(2)\phi(2)} \\ [A]_{S\times N}^{\phi(2)\psi(1)} & [A]_{S\times P}^{\phi(2)\phi(1)} & [A]_{S\times R}^{\phi(2)\psi(2)} & [A]_{S\times S}^{\phi(2)\phi(2)} \end{bmatrix} \quad (23)$$

and

$$\bar{c}_m = \begin{bmatrix} [a_m^{(1)}]_{N\times 1} \\ [b_m^{(1)}]_{P\times 1} \\ [a_m^{(2)}]_{R\times 1} \\ [b_m^{(2)}]_{S\times 1}\end{bmatrix} \quad (24)$$

$$\bar{d}_m = \begin{bmatrix} [d_m^{\psi(1)}]_{N\times 1} \\ [d_m^{\phi(1)}]_{P\times 1} \\ [d_m^{\psi(2)}]_{R\times 1} \\ [d_m^{\phi(2)}]_{S\times 1}\end{bmatrix}. \quad (25)$$

Each element of the submatrices of $\bar{\bar{A}}_m$ is given by

$$A_{mnp}^{\gamma(I)\chi(J)} = \int_0^{\infty} dk_\rho k_\rho \bar{\gamma}_{mn}^{(I)\dagger}(k_\rho)\cdot\bar{\bar{\xi}}_{I,J}(k_\rho, z_I', z_J')\cdot\bar{\chi}_{mp}^{(J)}(k_\rho) \quad (26)$$

where $\bar{\gamma}_{mn}^{(J)}(k_\rho)$ and $\bar{\chi}_{mn}^{(J)}(k_\rho)$ represent either $\bar{\psi}_{mn}^{(J)}(k_\rho)$ or $\bar{\phi}_{mn}^{(J)}(k_\rho)$. Each element of the excitation matrix $\bar{d}_m$ is given by

$$d_{mn}^{\gamma(I)} = -\int_0^{\infty} dk_\rho k_\rho \bar{\gamma}_{mn}^{(I)\dagger}(k_\rho)\cdot\bar{\bar{\xi}}_{I,3}^{TM}(k_\rho, z_I')\cdot\bar{p}_m(k_\rho) - \int_0^{\infty} dk_\rho k_\rho \gamma_{mn}^{(I)\dagger}(k_\rho)\cdot\bar{\bar{\xi}}_{I,2}(k_\rho, z_I', z_2')\cdot\bar{\kappa}_m^{(2,att)}(k_\rho). \quad (27)$$

IV. Input Impedance

Once the induced current distribution on the microstrip disks due to the coaxial probe excitation is solved for, the input impedance of the stacked microstrip antenna may be calculated. Applying (1), the input impedance for the stacked microstrip antenna is given by

$$Z_{in} = -\frac{1}{I^2}\int_{d_3}^{d_2} dz \int_0^{2\pi} d\phi_p \int_0^{\infty} d\rho_p \rho_p \{[\bar{E}_{3,1}(\bar{r})]_z + [\bar{E}_{3,2}(\bar{r})]_z + [\bar{E}_{self}(\bar{r})]_z\}\cdot\frac{I}{2\pi R}\delta(\rho_p - R) \quad (28)$$

where $\bar{E}_{3,j}(\bar{r})$ is the electric field due to disk current j and $\bar{E}_{self}(\bar{r})$ is the electric field due to the probe current. After integration over the cylindrical probe surface and some manipulation, we arrive at

$$\begin{aligned} Z_{in} &= -\frac{2\pi}{I^2}\sum_{m=-\infty}^{\infty}\int_0^{\infty} dk_\rho k_\rho p_m^*(k_\rho)\{\eta_{3,1}^{TM}(k_\rho) \\ &\quad \cdot\left[\bar{K}_m^{(1)}(k_\rho)\right]_\rho + \eta_{3,2}^{TM}(k_\rho)\left[\bar{K}_m^{(2)}(k_\rho)\right]_\rho\} + Z_{in}^{(self)} \\ &= -\frac{2\pi}{I^2}\sum_{m=-\infty}^{\infty}\int_0^{\infty} dk_\rho k_\rho p_m^*(k_\rho)\Bigg\{\eta_{3,1}^{TM}(k_\rho) \\ &\quad \cdot\sum_n^N a_{mn}^{(1)}\left[\bar{\psi}_{mn}^{(1)}(k_\rho)\right]_\rho + \eta_{3,1}^{TM}(k_\rho)\sum_p^P b_{mp}^{(1)} \\ &\quad \cdot\left[\bar{\phi}_{mp}^{(1)}(k_\rho)\right]_\rho + \eta_{3,2}^{TM}(k_\rho)\sum_r^R a_{mr}^{(2)}\left[\bar{\psi}_{mr}^{(2)}(k_\rho)\right]_\rho \\ &\quad + \eta_{3,2}^{TM}(k_\rho)\sum_s^S b_{ms}^{(2)}\left[\bar{\phi}_{ms}^{(2)}(k_\rho)\right]_\rho\Bigg\} + Z_{in}^{(self)} + Z_{in}^{(2,att)} \end{aligned} \tag{29}$$

where

$$\begin{aligned} \eta_{3,1}^{TM}(k_\rho) &= -\frac{\eta_1}{2}\frac{k_{1z}}{k_1} \\ &\quad \cdot\frac{\left[1-R_{\cap 1}^{TM}\right]\left[1-R_{\cap 2}^{TM}\right]\left[1-R_{U1}^{TM}e^{i2k_{3z}(d_0-z_1')}\right]}{\left[1-R_{U1}^{TM}R_{\cap 1}^{TM}e^{i2k_{1z}h_1}\right]\left[1-R_{\cap 2}^{TM}e^{i2k_{2z}h_2}\right]} \\ &\quad \cdot e^{ik_{1z}(z_1'-d_1)}e^{ik_{2z}h_2} \end{aligned} \tag{30}$$

$$\eta_{3,2}^{TM}(k_\rho) = -\frac{\eta_3}{2}\frac{k_{3z}}{k_3}\frac{\left[1-R_{U3}^{TM}\right]\left[1-e^{i2k_{3z}h_3}\right]}{\left[1-R_{U3}^{TM}e^{i2k_{3z}h_3}\right]} \tag{31}$$

and $\eta_l = \sqrt{\mu_l/\epsilon_l}$. The expressions for the generalized reflection coefficients R_{Ul}^{α} and $R_{\cap l}^{\alpha}$ are given in the Appendix. $Z_{in}^{(self)}$ represents the self-impedance of the probe and may be expressed as

$$\begin{aligned} Z_{in}^{(self)} &= \frac{\eta_3}{4}k_3h_3J_0(k_3R)H_0^{(1)}(k_3R) - \frac{1}{2\pi}\int_0^{\infty} \\ &\quad \cdot dk_\rho k_\rho J_0^2(k_\rho R)\left(\frac{k_\rho^2}{k_{3z}^4}\right)\eta_{3,2}^{TM}(k_\rho) \end{aligned} \tag{32}$$

$Z_{in}^{(2,att)}$ is the input impedance term due to the attachment mode and is given by

$$\begin{aligned} Z_{in}^{(2,att)} &= \frac{1}{2\pi}\int_0^{\infty} dk_\rho k_\rho J_0^2(k_\rho R)\left(\frac{k_\rho^2}{k_{3z}^4}\right)\eta_{3,2}^{TM}(k_\rho) \\ &\quad -\frac{1}{I}\sum_{m=-\infty}^{\infty} e^{-im\phi_0}\frac{J_0(k_3R)J_m(k_3\rho_0)}{J_m'(k_3a_2)}\int_0^{\infty} \\ &\quad \cdot dk_\rho k_\rho p_m^*(k_\rho)J_m'(k_\rho a_2)\left(\frac{k_3}{k_{3z}^2}\right)\eta_{3,2}^{TM}(k_\rho). \end{aligned} \tag{33}$$

The first term of the probe self-impedance in (32) corresponds to the input impedance of a coaxial probe driven parallel-plate waveguide. In the small k_3R limit, this term reduces to

$$\begin{aligned} &\lim_{k_3R\to 0}\frac{\eta_3}{4}k_3h_3J_0(k_3R)H_0^{(1)}(k_3R) \\ &\quad = i\frac{\eta_0}{2\pi}k_0h_3\frac{\mu_3}{\mu_0}\ln(k_3R) = i60k_0h_3\frac{\mu_3}{\mu_0}\ln(k_3R) \end{aligned}$$

which is the formula used by some authors as the probe reactance [24]. Upon careful inspection of the expression for the probe self-impedance $Z_{in}^{(self)}$, it is noted that the second term in (32) containing $\eta_{3,2}^{TM}(k_\rho)$ is zero when R_{U3}^{TM} is equal to one—the case of a probe-fed parallel plate waveguide. When R_{U3}^{TM} is not equal to one, this term diverges. This is because the uniform current on the probe leads to a singular charge accumulation at the probe end giving rise to a singular reactance. Thus, in the case of a microstrip disk excited by a probe, in order to account properly for the probe-self impedance, the continuity of the current at the probe-disk junction must be ensured. If we take the impedance due to the probe and the attachment mode current together, we arrive at the following:

$$\begin{aligned} &Z_{in}^{(self)} + Z_{in}^{(2,att)} \\ &\quad = \frac{\eta_3}{4}k_3h_3J_0(k_3R)H_0^{(1)}(k_3R) \\ &\quad\quad -\frac{1}{I}\sum_{m=-\infty}^{\infty} e^{-im\phi_0}\frac{J_0(k_3R)J_m(k_3\rho_0)}{J_m'(k_2a_2)} \\ &\quad\quad \cdot\int_0^{\infty} dk_\rho k_\rho p_m^*(k_\rho)J_m'(k_\rho a_2)\left(\frac{k_3}{k_{3z}^2}\right)\eta_{3,2}^{TM}(k_\rho) \end{aligned} \tag{34}$$

where the divergent term in the probe self-impedance $Z_{in}^{(self)}$ has been cancelled by the contribution of the attachment mode which ensures continuity of the current.

V. Radiation Fields

The radiation field, or far field, components in region 0 may be obtained from the longitudinal components with:

$$E_{0\phi} = \frac{\eta_0 H_{0z}}{\sin\theta} \quad E_{0\theta} = -\frac{E_{0z}}{\sin\theta}. \tag{35}$$

For large observation distances, the expressions for the field components may be evaluated using the saddle point method with the saddle point being $k_\rho = k_0\sin\theta$ where $\theta = \tan^{-1}(\rho/z)$. The longitudinal field components due to disk current $\bar{K}_j(\bar{\rho})$ are given by

$$\begin{aligned} E_{0z}^{(j)}(\bar{\rho},z) &= \sum_{m=-\infty}^{\infty} e^{im\phi}(-i)^m\{k_\rho e_{0,j}(k_\rho,z_j') \\ &\quad \cdot\left[\bar{\kappa}_m^{(j)}(k_\rho)\right]_\rho\}_{k_\rho=k_0\sin\theta}\frac{e^{ik_0r}}{r} \end{aligned} \tag{36a}$$

$$\begin{aligned} H_{0z}^{(j)}(\bar{\rho},z) &= \sum_{m=-\infty}^{\infty} e^{im\phi}(-i)^m\{k_\rho h_{0,j}(k_\rho,z_j') \\ &\quad \cdot\left[\bar{\kappa}_m^{(j)}(k_\rho)\right]_\phi\}_{k_\rho=k_0\sin\theta}\frac{e^{ik_0r}}{r} \end{aligned} \tag{36b}$$

where

$$e_{0,1}(k_\rho, z_1') = \frac{\eta_1}{2}\frac{k_{1z}}{k_1} \cdot \frac{\left[1 - R_{U1}^{TM}\right]\left[1 - R_{\cap 1}^{TM} e^{i2k_{1z}(z_1 - d_1)}\right]}{1 - R_{U1}^{TM} R_{\cap 1}^{TM} e^{i2k_{1z}h_1}} \cdot e^{ik_{1z}(d_0 - z_1)} e^{-ik_{0z}d_0} \quad (37a)$$

$$h_{0,1}(k_\rho, z_1') = -\frac{\mu_1}{\mu_0}\frac{k_{0z}}{k_{1z}} \cdot \frac{\left[1 + R_{U1}^{TE}\right]\left[1 + R_{\cap 1}^{TE} e^{i2k_{1z}(z_1 - d_1)}\right]}{1 - R_{U1}^{TE} R_{\cap 1}^{TE} e^{i2k_{1z}h_1}} \cdot e^{-ik_{0z}d_0} e^{ik_{1z}(d_0 - z_1)} \quad (37b)$$

$$e_{0,2}(k_\rho, z_2') = \frac{\eta_2}{2}\frac{k_{2z}}{k_2} \cdot \frac{\left[1 - R_{U1}^{TM}\right]\left[1 - R_{U2}^{TM}\right]\left[1 - R_{\cap 2}^{TM}\right]}{\left[1 - R_{U2}^{TM} R_{\cap 2}^{TM} e^{i2k_{2z}h_2}\right]\left[1 - R_{U1}^{TM} e^{i2k_{1z}h_1}\right]} \cdot e^{-ik_{0z}d_0} e^{ik_{1z}h_1} e^{ik_{2z}h_2} \quad (37c)$$

$$h_{0,2}(k_\rho, z_2') = -\frac{\mu_2}{\mu_0}\frac{k_{0z}}{k_{2z}} \cdot \frac{\left[1 + R_{U1}^{TE}\right]\left[1 + R_{U2}^{TE}\right]\left[1 + R_{\cap 2}^{TE}\right]}{\left[1 - R_{U2}^{TE} R_{\cap 2}^{TE} e^{i2k_{2z}h_2}\right]\left[1 + R_{U1}^{TE} e^{i2k_{1z}h_1}\right]} \cdot e^{-ik_{0z}d_0} e^{ik_{1z}h_1} e^{ik_{2z}h_2}. \quad (37d)$$

Likewise, the radiation field component due to the probe is given by

$$E_{0z}^{P}(\bar{\rho}, z) = \sum_{m=-\infty}^{\infty} e^{im\phi}(-i)^m \cdot \left\{\frac{k_\rho}{k_{3z}} e_{0,3}^{P}(k_\rho) p_m(k_\rho)\right\}_{k_\rho = k_0 \sin\theta} \frac{e^{ik_0 r}}{r} \quad (38)$$

where

$$e_{0,3}^{P}(k_\rho) = \frac{\eta_3}{2}\frac{k_{3z}}{k_3} \frac{\left[1 - R_{U1}^{TM}\right]\left[1 - R_{U2}^{TM}\right]\left[1 - R_{U3}^{TM}\right]\left[1 - e^{i2k_{3z}h_3}\right]}{\left[1 - R_{U3}^{TM} e^{i2k_{3z}h_3}\right]\left[1 - R_{U1}^{TM} e^{i2k_{1z}h_1}\right]\left[1 - R_{U2}^{TM} e^{i2k_{2z}h_2}\right]} e^{-ik_{0z}d_0} e^{ik_{1z}h_1} e^{ik_{2z}h_2}. \quad (39)$$

VI. Numerical Results and Discussion

The integrals of the matrix elements, (26) and (27), and in the impedance expression (29), are evaluated numerically along an integration path deformed below the real axis to avoid the singularities on the real axis which correspond to the radiating and guided modes of the layered medium. When using cavity mode basis functions, the integrands vary asymptotically as $1/k_\rho^3$ while those using the Chebyshev polynomial basis functions with the edge condition vary asymptotically as $1/k_\rho^2$. To enhance the convergence of the integrals when using the Chebyshev polynomial basis functions, the asymptotic values of the integrands are subtracted out and evaluated analytically.

For the stacked microstrip configurations discussed here, the following parameters are used: $a_2 = 1.3233$ cm, $h_3 = 2h_1 = 0.115a_2$, $\epsilon_1 = \epsilon_3 = 2.45\epsilon_0$, $\epsilon_2 = 1.22\epsilon_0$ (foam), $\rho_0 = 0.6a_2$, and $R = 0.048a_2$. Given these parameters, the antenna is characterized by varying the upper radius a_1 and the separation between the disks h_2. Convergent results for the input impedance and radiation fields using cavity mode basis functions are obtained with ($N = 4, P = 3$), ($R = 4, S = 3$), while those using the Chebyshev polynomial basis functions with the edge condition use ($N = 3, P = 3$), ($R = 3, S = 3$). For the calculation of the input impedance given by (29), very good results are obtained with $m = \pm 1$ for the terms associated with the disk current amplitudes, $a_{mn}^{(1)}$, $b_{mp}^{(1)}$, $a_{mr}^{(2)}$, and $b_{ms}^{(2)}$, and taking $m = 0, \pm 1, \pm 2$ for the probe self-impedance and attachment mode terms in (34). Additional modes produce only a 1 or 2 Ω difference in the input impedance calculations for the parameters considered here. It is found numerically that the probe self-impedance and attachment mode impedance terms taken together in (34) give rise to a primarily inductive reactance contribution. Computation time for the input impedance of the stacked structure is approximately a half-hour of CPU time per frequency on a VAXstation 3500.

Calculated and measured [6] reflection coefficients, $\Gamma = (Z_{in} - Z_0)/(Z_{in} + Z_0)$ where $Z_0 = 50$ Ω, are shown in Figs. 2(a) and 2(b) for the stacked configuration case A with $a_1/a_2 = 1.01$ and h_2/a_2 equal to 0.36 and 0.48, respectively. The agreement between the measured and calculated results is very good. The loop in the impedance locus of Fig. 2(a) reduces in size in Fig. 2(b) as h_2/a_2 is increased from 0.36 to 0.48, leading to the wide bandwidth behavior of this configuration. Especially off resonance, it is seen that the attachment mode and probe self-impedance terms are required for accurate results.

In Fig. 3, return loss calculations using both cavity mode and Chebyshev polynomial basis functions are compared with measured results [6] for the case of Fig. 2(b). The agreement between the calculated and measured results is very good. A frequency shift in the results on the order of 1–2% is observed for the two sets of basis functions. Due to the presence of the upper disk in the stacked configurations, two resonances associated with the two constitutive resonators of the stacked structure [11] are easily distinguished, giving rise to a 16 % −15 dB bandwidth in this case. One resonance is associated with the resonator formed by the lower disk and the ground plane and the second resonance is associated with the resonator formed by the two disks. Comparing the return loss of the stacked configuration to that of the single disk, when the upper disk and substrate are removed, it is shown that the input impedance of the single disk presents an impedance mismatch. When the probe position is changed from $0.6a_2$ to approximately $0.3a_2$ to obtain a match, a 2.3%—10 dB bandwidth is achieved.

Fig. 4 illustrates the effect of the separation h_2/a_2 on the input impedance for the cases $a_1/a_2 = 1.05$, where the impedance has been calculated using the Chebyshev polynomial basis functions including the probe self-impedance and attachment mode terms. While the position of the lower resonance remains essentially the same, the position of the upper resonance is a function of the height h_2, decreasing with increasing h_2. As seen in the figure, the excitation of the upper resonance increases with increasing h_2 (up to a certain h_2 beyond which there is little coupling [11]). This is due to the fact that the coupling interaction between the two modes increases as the

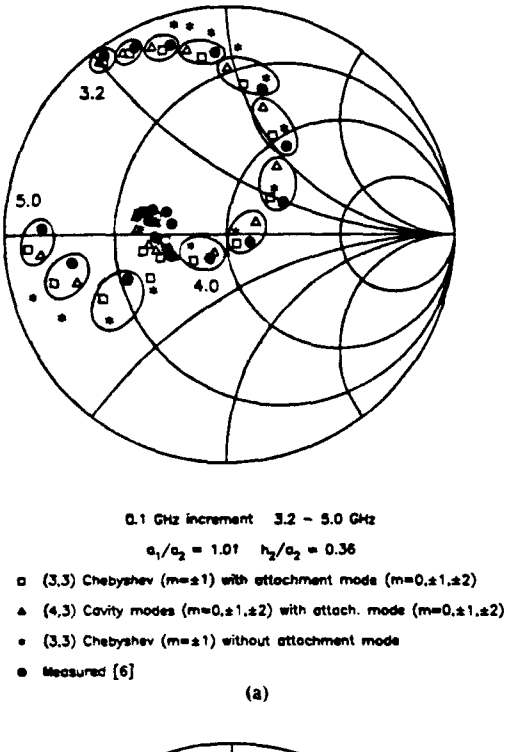

(a)

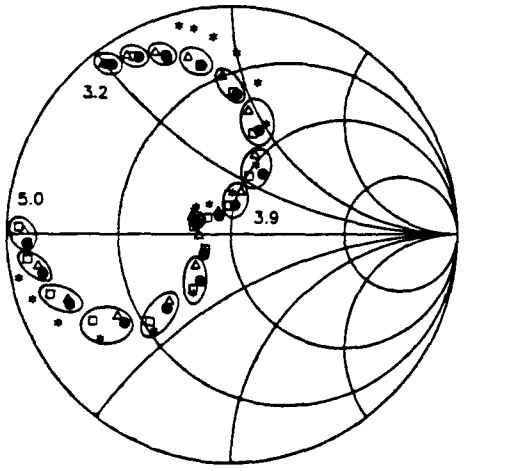

(b)

Fig. 2. Γ of stacked configuration A. $a_1/a_2 = 1.01$. (a) $h_2/a_2 = 0.36$. (b) $h_2/a_2 = 0.48$.

upper resonant frequency approaches the lower resonant frequency, i.e., as the upper resonant frequency decreases with increasing h_2. Or, conversely, the coupling interaction decreases as the separation between the disks approaches zero. Calculated and measured [6] return loss results are compared in Fig. 5, where a 13%—10 dB bandwidth is obtained in Fig. 5(a) and where dual frequency operation is observed in Fig. 5(b). Again, the agreement between the calculated and measured results is good.

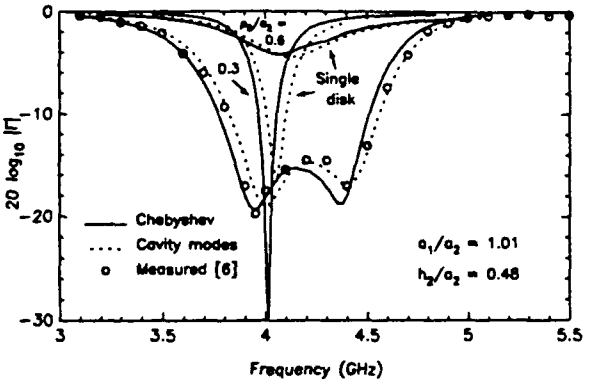

Fig. 3. Return loss of stacked configuration A. $a_1/a_2 = 1.01$ and $h_2/a_2 = 0.48$. Return loss of single disk with no upper substrate and $\rho_0/a_2 = 0.3,0.6$.

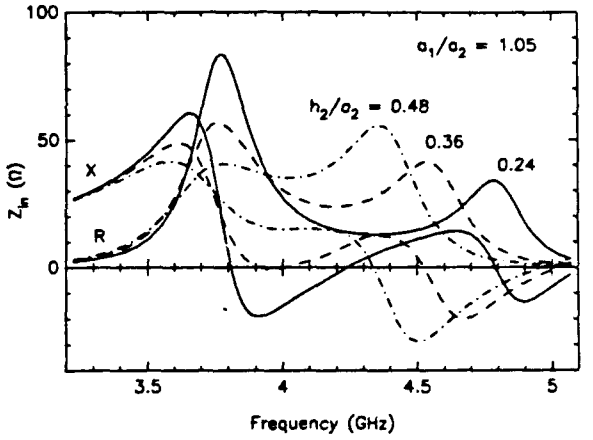

Fig. 4. Input impedance of stacked configuration A. $a_1/a_2 = 1.05$ and $h_2/a_2 = 0.24$ (—), 0.36 (- -), 0.48 (-·-).

Shown in Fig. 6 are the input impedance results of configurations A and B with parameters $a_1/a_2 = 1.2$ and $h_2/a_2 = 0.24$. Generally, the two configurations have similar characteristics. For configuration B, the increased distance between the two disks and the higher "effective" dielectric constant between the disks results in an upper resonance occurring at a lower frequency as compared with configuration A.

Illustrated in Fig. 7 are the disk current distributions for configuration A with $a_1/a_2 = 1.01$ and $h_2/a_2 = 0.48$ at the lower resonance, that is with $k_3a_2 = 1.655$ using (4,4) Chebyshev basis functions for each disk and $k_3a_2 = 1.68$ using (5,4) cavity mode basis functions for each disk. As the number of cavity mode basis functions is increased, the singular behavior at the disk edge of the $\hat{\phi}$ component of the current distribution is better characterized. The magnitude of the $\hat{\phi}$ component of the current for the upper disk is approximately uniform across the disk where the amplitude slightly increases toward the edges due to the parasitic effect of the upper disk excited by the fringing fields.

In Fig. 8, the radiation patterns of the stacked microstrip antenna configuration of Fig. 7 are compared with those of the single disk with no upper substrate. For the probe-fed single microstrip disk, the probe position is taken to be $\rho_0/a_2 = 0.3$, while $\rho_0/a_2 = 0.6$ for the stacked configuration. The E_ϕ component remains essentially the same for both the single disk and stacked configuration. The radiation pattern of the stacked con-

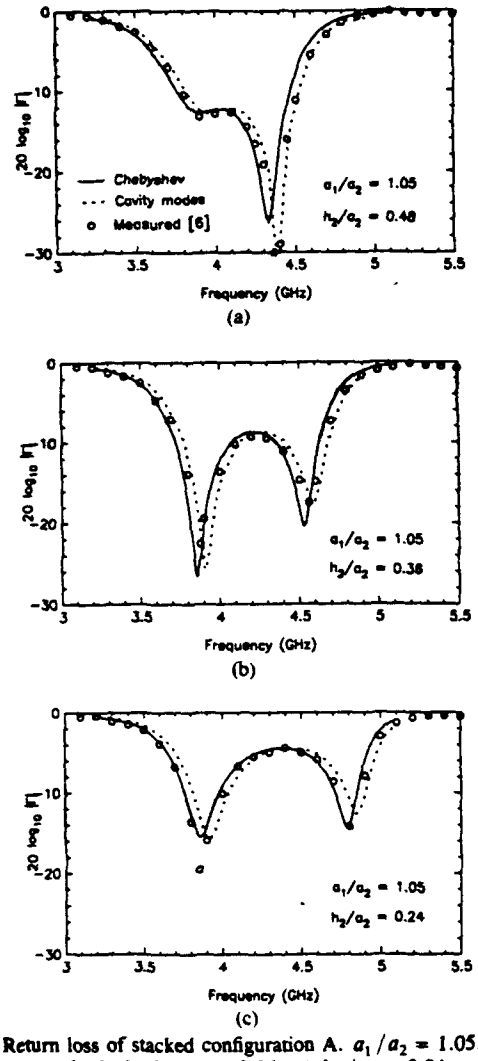

Fig. 5. Return loss of stacked configuration A. $a_1/a_2 = 1.05$. (a) $h_2/a_2 = 0.48$. (b) $h_2/a_2 = 0.36$. (c) $h_2/a_2 = 0.24$.

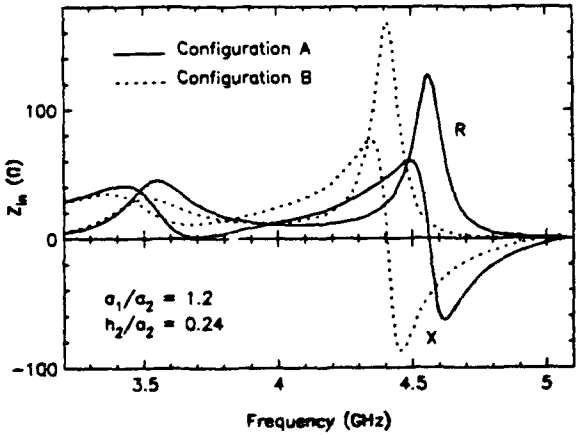

Fig. 6. Input impedance of stacked configurations A and B. $a_1/a_2 = 1.2$ and $h_2/a_2 = 0.24$.

figuration is more directive than that of the single disk, where the E_θ beamwidth is decreased in the stacked case.

VII. Conclusion

The input impedance of a microstrip antenna consisting of two circular microstrip disks in a stacked configuration driven by a coaxial probe is investigated. A rigorous analysis is performed using a dyadic Green's function formulation where the mixed boundary value problem is reduced to a set of coupled vector integral equations using the vector Hankel transform. Galerkin's method is employed in the spectral domain with an additional term used in the current expansion to account for the singular nature of the current in the vicinity of the probe, ensure continuity of the current, and to speed up convergence of the solution. Ensuring continuity of the current by means of the attachment mode is shown to be necessary for rigorously including the

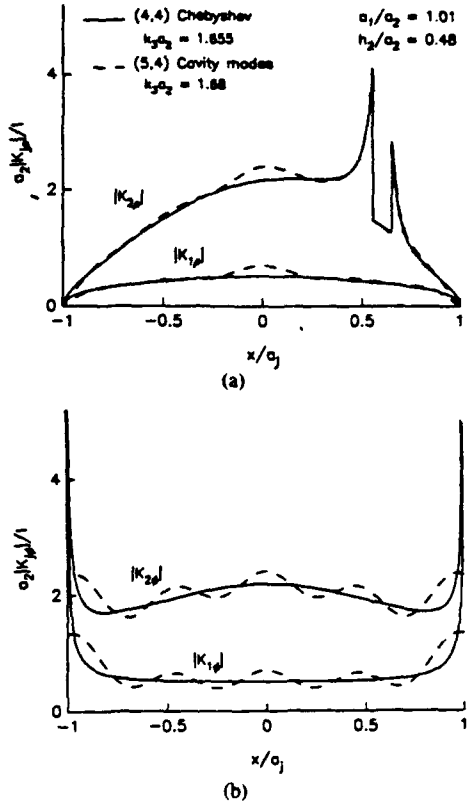

Fig. 7. Disk currents of stacked configuration A. $a_1/a_2 = 1.01$, $h_2/a_2 = 0.48$. (a) $a_2|K_{j\rho}/I|$. (b) $a_2|K_{j\phi}/I|$.

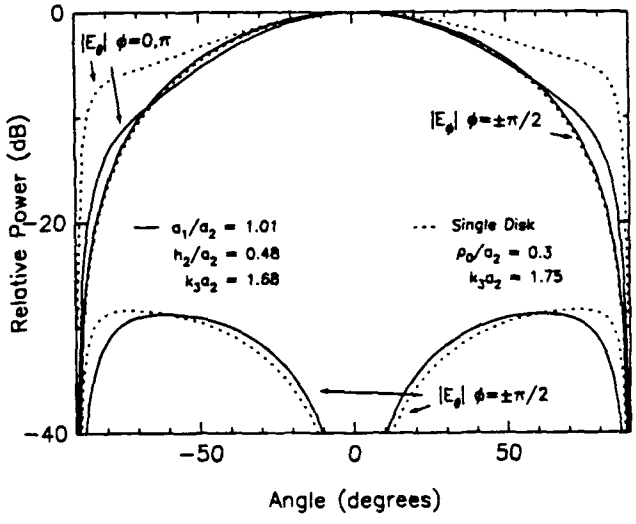

Fig. 8. Radiation pattern for stacked configuration A (—) with $a_1/a_2 = 1.01$, $h_2/a_2 = 0.48$, $k_3a_2 = 1.68$, and for single disk ($\cdots$) with $k_3a_2 = 1.75$ and $\rho_0/a_2 = 0.3$.

probe self-impedance and obtaining accurate results for the stacked microstrip configuration. The input impedance of the stacked microstrip antenna is calculated as a function of the layered parameters and the ratio of the two disks. Both wide bandwidth and dual frequency operation are shown. Disk current distributions and radiation patterns are also presented. Calculated results for the stacked microstrip configuration are shown to compare well with experimental data.

VIII. Appendix

The explicit expressions for $\xi_{i,3}^{TM}(k_\rho, z)$, $\xi_{i,j}^{TM}(k_\rho, z, z')$, and $\xi_{i,j}^{TE}(k_\rho, z, z')$ of (11) and (12) are given here. For the stacked configurations of Fig. 1, we have

$$\xi_{2,3}^{TM}(k_\rho, z_2') = -\frac{\eta_3}{2}\frac{k_{3z}}{k_3} \cdot \frac{\left[1 - R_{U3}^{TM}\right]\left[1 + R_{\cap 3}^{TM} e^{ik_{3z}h_3}\right]\left[1 - e^{ik_{3z}h_3}\right]}{\left[1 - R_{U3}^{TM} R_{\cap 3}^{TM} e^{i2k_{3z}h_3}\right]} \tag{40}$$

$$\xi_{1,3}^{TM}(k_\rho, z_1') = \xi_{2,3}^{TM}(k_\rho, z_2') \cdot \frac{\left[1 - R_{U2}^{TM}\right]\left[1 - R_{U1}^{TM} e^{i2k_{1z}(d_0 - z_1')}\right]}{\left[1 - R_{U1}^{TM} e^{i2k_{1z}h_1}\right]\left[1 - R_{U2}^{TM} e^{i2k_{2z}h_2}\right]} \cdot e^{ik_{1z}(z_1' - d_1)} e^{ik_{2z}h_2} \tag{41}$$

where $\eta_l = \sqrt{\mu_l/\epsilon_l}$ and $z_2' = d_2$.

For source and observer are in region 1 (assuming $z > z'$), the expressions are

$$\xi_{1,1}^{TM}(k_\rho, z, z') = -\frac{\eta_1}{2}\frac{k_{1z}}{k_1}\frac{\left[1 - R_{U1}^{TM} e^{i2k_{1z}(d_0 - z)}\right]\left[1 - R_{\cap 1}^{TM} e^{i2k_{1z}(z' - d_1)}\right]}{1 - R_{U1}^{TM} R_{\cap 1}^{TM} e^{i2k_{1z}h_1}} e^{ik_{1z}(z - z')} \tag{42a}$$

$$\xi_{1,1}^{TE}(k_\rho, z, z') = -\frac{\eta_1}{2}\frac{k_1}{k_{1z}}\frac{\left[1 + R_{U1}^{TE} e^{i2k_{1z}(d_0 - z)}\right]\left[1 + R_{\cap 1}^{TE} e^{i2k_{1z}(z' - d_1)}\right]}{1 - R_{U1}^{TE} R_{\cap 1}^{TE} e^{i2k_{1z}h_1}} e^{ik_{1z}(z - z')}. \tag{42b}$$

For an observer in region 2 and source in region 1, the expressions are

$$\xi_{2,1}^{TM}(k_\rho, z, z') = -\frac{\eta_1}{2}\frac{k_{1z}}{k_1}\frac{\left[1 - R_{\cap 1}^{TM}\right]\left[1 - R_{\cap 2}^{TM} e^{i2k_{2z}(z - d_2)}\right]\left[1 - R_{U1}^{TM} e^{i2k_{1z}(d_0 - z')}\right]}{\left[1 - R_{U1}^{TM} R_{\cap 1}^{TM} e^{i2k_{1z}h_1}\right]\left[1 - R_{\cap 2}^{TE} e^{i2k_{2z}h_2}\right]} e^{ik_{1z}(z' - d_1)} e^{ik_{2z}(d_1 - z)} \tag{43a}$$

$$\xi_{2,1}^{TE}(k_\rho, z, z') = -\frac{\eta_1}{2}\frac{k_1}{k_{1z}}\frac{\left[1 + R_{\cap 1}^{TE}\right]\left[1 + R_{\cap 2}^{TE} e^{i2k_{2z}(z - d_2)}\right]\left[1 + R_{U1}^{TE} e^{i2k_{1z}(d_0 - z')}\right]}{\left[1 - R_{U1}^{TE} R_{\cap 1}^{TE} e^{i2k_{1z}h_1}\right]\left[1 + R_{\cap 2}^{TE} e^{i2k_{2z}h_2}\right]} e^{ik_{1z}(z' - d_1)} e^{ik_{2z}(d_1 - z)} \tag{43b}$$

By reciprocity, $\xi_{1,2}^{\alpha}(k_\rho, z, z') = \xi_{2,1}^{\alpha}(k_\rho, z', z)$ (α = TM,TE). For source and observer in region 2 (assuming $z > z'$), the expressions are

$$\xi_{2,2}^{TM}(k_\rho, z, z') = -\frac{\eta_2}{2}\frac{k_{2z}}{k_2}\frac{\left[1 - R_{U2}^{TM} e^{i2k_{2z}(d_1 - z)}\right]\left[1 - R_{\cap 2}^{TM} e^{i2k_{2z}(z' - d_2)}\right]}{1 - R_{U2}^{TM} R_{\cap 2}^{TM} e^{i2k_{2z}h_2}} e^{ik_{2z}(z - z')} \tag{44a}$$

$$\xi_{2,2}^{TE}(k_\rho, z, z') = -\frac{\eta_2}{2}\frac{k_2}{k_{2z}}\frac{\left[1 + R_{U2}^{TE} e^{i2k_{2z}(d_1 - z)}\right]\left[1 + R_{\cap 2}^{TE} e^{i2k_{2z}(z' - d_2)}\right]}{1 - R_{U2}^{TE} R_{\cap 2}^{TE} e^{i2k_{2z}h_2}} e^{ik_{2z}(z - z')} \tag{44b}$$

The generalized reflection coefficients, R_{Ul}^{α} and $R_{\cap l}^{\alpha}$, at the upper and lower boundaries, respectively, of layer l, are given by the following recursion relations

$$R_{Ul}^{\alpha} = \frac{R_{l(l-1)}^{\alpha} + R_{U(l-1)}^{\alpha} e^{i2k_{(l-1)z}h_{l-1}}}{1 + R_{l(l-1)}^{\alpha} R_{U(l-1)}^{\alpha} e^{i2k_{(l-1)z}h_{l-1}}} \tag{45a}$$

$$R_{\cap l}^{\alpha} = \frac{R_{l(l+1)}^{\alpha} + R_{\cap(l+1)}^{\alpha} e^{i2k_{(l+1)z}h_{l+1}}}{1 + R_{l(l+1)}^{\alpha} R_{\cap(l+1)}^{\alpha} e^{i2k_{(l+1)z}h_{l+1}}} \tag{45b}$$

where $R_{U0}^{TE} = R_{U0}^{TM} = 0$ and $R_{\cap 3}^{TE} = -1$ and $R_{\cap 3}^{TM} = 1$. The Fresnel reflection coefficients $R_{l(l\pm1)}^{TE}$ and $R_{l(l\pm1)}^{TM}$ are defined by

$$R_{l(l\pm1)}^{TE} = \frac{\mu_{(l\pm1)}k_{lz} - \mu_l k_{(l\pm1)z}}{\mu_{(l\pm1)}k_{lz} + \mu_l k_{(l\pm1)z}} \tag{45a}$$

$$R_{(l\pm1)}^{TM} = \frac{\epsilon_{(l\pm1)}k_{lz} - \epsilon_l k_{(l\pm1)z}}{\epsilon_{(l\pm1)}k_{lz} + \epsilon_l k_{(l\pm1)z}}. \tag{46b}$$

Acknowledgment

The authors would like to acknowledge and express their gratitude to Dr. Robert M. Sorbello at COMSAT Laboratories for providing the opportunity to perform the experimental work. We would also like to thank Henry B. Williams for his laboratory assistance.

References

[1] K. R. Carver and J. W. Mink, "Microstrip antenna technology," *IEEE Trans. Antennas Propagat.*, vol. AP-29, pp. 2-23, Jan. 1981.

[2] H. G. Oltman, "Electromagnetically coupled microstrip dipole antenna elements," in *Proc. 8th European Microwave Conf.*, Paris, 1977, pp. 281-285.

[3] P. S. Hall, C. Wood, and C. Garrett, "Wide bandwidth microstrip antennas for circuit integration," *Electron. Lett.*, vol. 15, no. 15, p. 458-460, 19 July 1979.

[4] A. Sabban, "A new broadband stacked two-layer microstrip antenna," in *1983 IEEE Antennas Propagat. Soc. Int. Symp. Dig.*, June 1983, pp. 63-66.

[5] C. H. Chen, A. Tulintseff, and R. M. Sorbello, "Broadband two-layer microstrip antenna," in *1984 IEEE Antennas Propagat. Soc. Int. Symp. Dig.*, June 1984, pp. 251-254.

[6] A. N. Tulintseff, "Experiment and analysis of a circularly polarized electromagnetically coupled microstrip antenna," S.M. thesis, Massachusetts Inst. Technol., Cambridge, MA, Feb. 1985.

[7] R. Q. Lee, K. F. Lee, and J. Bobinchak, "Characteristics of a two-layer electromagnetically coupled rectangular patch antenna," *Electron. Lett.*, vol. 23, no. 20, pp. 1070-1073, Sept. 24, 1987.

[8] S. A. Long and M. D. Walton, "A dual-frequency stacked circular-disc antenna," *IEEE Trans. Antennas Propagat.*, vol. AP-27, pp. 270-273, Mar. 1979.

[9] J. S. Dahele, K.-F. Lee, and D. P. Wong, "Dual-frequency stacked annular-ring microstrip antenna," *IEEE Trans. Antennas Propagat.*, vol. AP-35, pp. 1281-1285, Nov. 1987.

[10] K. Araki, H. Ueda, and T. Masayuki, "Numerical analysis of circular disk microstrip antennas with parasitic elements," *IEEE Trans. Antennas Propagat.*, vol. AP-34, pp. 1390-1394, Dec. 1986.

[11] A. N. Tulintseff, S. M. Ali, and J. A. Kong, "Resonant frequencies of stacked circular microstrip antennas," submitted for publication.

[12] A. N. Tulintseff and R. M. Sorbello, "Current and radiation fields of electromagnetically coupled microstrip antennas," in *1987 IEEE Int. Symp. Dig., Antennas Propagat.*, vol. 2, June 1987, pp. 928-931.

[13] R. Kastner, E. Heyman, and A. Sabban, "Spectral domain iterative analysis of single- and double-layered microstrip antennas using the conjugate gradient algorithm," *IEEE Trans. Antennas Propagat.*, vol. 36, pp. 1204-1212, Sept. 1988.

[14] A. Reineix and B. Jecko, "Analysis of microstrip patch antennas using finite difference time domain method," *IEEE Trans. Antennas Propagat.*, vol. 37, pp. 1361-1369, Nov. 1989.

[15] S. Yano and A. Ishimaru, "A theoretical study of the input impedance of a circular microstrip disk antenna," *IEEE Trans. Antennas Propagat.*, vol. AP-29, pp. 77-83, Jan. 1981.

[16] W. C. Chew and J. A. Kong, "Analysis of a circular microstrip disk antenna with a thick dielectric substrate," *IEEE Trans. Antennas Propagat.*, vol. AP-29, pp. 68-76, Jan. 1981.

[17] S. M. Ali, W. C. Chew, and J. A. Kong, "Vector Hankel transform analysis of annular-ring microstrip antenna," *IEEE Trans. Antennas Propagat.*, vol. AP-30, pp. 637-644, July 1982.

[18] T. M. Habashy, J. A. Kong, and W. C. Chew, "Resonance and radiation of the elliptic disk microstrip structure, Part I: Formulation," *IEEE Trans. Antennas Propagat.*, vol. AP-35, pp. 877-886, Aug. 1987.

[19] D. M. Pozar, "Input impedance and mutual coupling of rectangular microstrip antennas," *IEEE Trans. Antennas Propagat.*, vol. AP-23, pp. 1191-1196, Nov. 1982.

[20] T. M. Habashy, S. M. Ali, and J. A. Kong, "Impedance parameters and radiation pattern of two coupled circular microstrip disk antennas," *J. Math. Phys.*, vol. 54, no. 2, pp. 493-506, Feb. 1983.

[21] K. R. Carver, "Input impedance to probe-fed microstrip antennas," in *1980 IEEE Int. Symp. Dig.—Antennas Propagat.*, vol. 2, June 1980, pp. 617-620.

[22] J. T. Aberle and D. M. Pozar, "Analysis of infinite arrays of probe-fed rectangular microstrip patches using a rigorous feed model," *Proc. Inst. Elec. Eng.*, vol. 136, pt. H, no. 2, pp. 110-119, Apr. 1989.

[23] M. A. Blischke, E. J. Rothwell, and K. M. Chen, "Receiving and scattering characteristics of circular patch antenna array," *J. Electromagn. Waves Appl.*, vol. 2, no. 3/4, pp. 353-378, 1988.

[24] M. C. Bailey and M. D. Deshpande, "Analysis of elliptical and circular microstrip antennas using moment method," *IEEE Trans. Antennas Propagat.*, vol. AP-33, pp. 9054-9059, Sept. 1985.

[25] S. Pinhas, S. Shtrikman, and D. Treves, "Moment-method solution of the center-fed microstrip disk antenna invoking feed and edge current singularities," *IEEE Trans. Antennas Propagat.*, vol. 37, pp. 1516-1522, Dec. 1989.

[26] M. Davidovitz and Y. T. Lo, "Input impedance of a probe-fed circular microstrip antenna with thick substrate," *IEEE Trans. Antennas Propagat.*, vol. AP-34, pp. 905-911, July 1986.

[27] W. L. Weeks, *Antenna Engineering*. New York: McGraw-Hill, 1968.

[28] W. C. Chew and T. M. Habashy, "The use of vector transforms in solving some electromagnetic scattering problems," *IEEE Trans. Antennas Propagat.*, vol. AP-34, pp. 871-879, July 1986.

[29] I. S. Gradshteyn and I. M. Ryzhik, *Table of Integrals, Series, and Products*. New York: Academic, 1965.

[30] M. Abramowitz and I. A. Stegun, *Handbook of Mathematical Functions*. Nat. Bur. Stand., 1964.

Ann N. Tulintseff was born in Seattle, WA, on April 23, 1961. She received the S.B., S.M., and Ph.D. degrees from the Massachusetts Institute of Technology, Cambridge, in 1985 and 1990, respectively.

During her graduate work, she held both Teaching and Research Assistantships. In 1986, she received the Frederick C. Hennie III Award for Excellence in Teaching and was appointed the position Instructor-G in the Department of Electrical Engineering and Computer Science. Her area of interest is electromagnetic wave theory and applications, with particular interest in microstrip antennas, microwave and millimeter wave antennas and circuit components, and wave propagation in layered media.

Dr. Tulintseff is a member of Eta Kappa Nu and Tau Beta Pi.

Sami M. Ali (M'79-SM'86), for a photograph and biography please see page 731 of the May 1990 issue of this TRANSACTIONS.

Jin Au Kong (S'65-M'69-SM'74-F'85), for a photograph and biography please see page 1149 of the September 1989 issue of this TRANSACTIONS.

Journal of Electromagnetic Waves and Applications, Vol. 3, No. 3, 183-197, 1989

Transient Analysis of Frequency-Dependent Transmission Line Systems Terminated with Nonlinear Loads

Q. Gu

Shanghai Xinhua Radio Factory
Shanghai, PRC

Y. E. Yang and J. A. Kong

Department of Electrical Engineering and Computer Science
and Research Laboratory of Electronics
Massachusetts Institute of Technology
Cambridge, MA 02139, USA

Abstract– A new method for analyzing frequency-dependent transmission line systems with nonlinear terminations is presented. The generalized scattering matrix formulation is used as the foundation for the time domain iteration scheme. Compared to the admittance matrix approach proposed in a previous paper, it has the advantage of shorter impulse response which leads to smaller computer memory requirement and faster computation time. Examples of a microstrip line loaded with nonlinear elements are given to illustrate the efficiency of this method.

I. INTRODUCTION

In recent years, the effect of the interconnection lines on high-speed integrated circuits has become more and more important. As the speeds of integrated circuits increase, the propagation delay as well as the dispersion and loss of interconnection lines can no longer be neglected. Traditional lumped element circuit models must be supplemented by dispersive transmission line models in order to account for these effects. This has created the need for new numerical procedures that can be easily incorporated into current CAD tools. To make matters more complicated, the interconnection lines are terminated with not only linear elements but also nonlinear semiconductor devices, such as diodes and transistors.

Several techniques are now commonly used to deal with nonlinear circuit problems, for example, the direct time domain approaches [1,2], and the semi-frequency domain approaches, such as the harmonic balance [3,4] and the modified harmonic balance techniques [5,6]. Semi-frequency domain approaches are useful for microwave and millimeter wave integrated circuits but become impractical for digital integrated circuits because of their wide-band nature. On the other hand, frequency-dependent parameters often make it awkward to apply the direct time domain approach to interconnection line systems. The time-domain finite-difference method [7] and the time-domain method of moments [8] have been proposed to deal directly with electromagnetic scattering from nonlinear loads.

However, dispersion problems are absent from the discussions.

Liu and Tesche [1] developed a combined time-domain frequency-domain treatment of antennas and scatterers with nonlinear loads. In their work, the transfer function (impulse response) of the linear portion of the investigated system is first obtained through the frequency-domain analysis, and it is then used to solve the entire nonlinear problem in the time domain. Subsequent improvements to this method have been suggested by Djordjevic, Sarkar and Harrington [9] through artificially introducing pairs of quasi-matched passive networks, and by Caniggia [10] and Schutt-Aine and Mittra [11], through macromodel and scattering parameter analysis based on a fixed reference impedance.

In this paper we shall present an extended and more natural method that will completely eliminate the need for any artificial networks or fixed reference impedances. Its close ties to the physics of transmitted and reflected waves on transmission lines also help in achieving the purpose of reducing computation time. The algorithm is explained in the next section. In Section III the details of applying our formulations to frequency-dependent transmission lines with nonlinear loads are illustrated in the analyses of a nonlinearly-loaded dispersive transmission line.

II. ANALYSIS BASED ON WAVE TRANSMISSION AND REFLECTION

An arbitrary system of n dispersive transmission lines can be represented by the following coupled linear ordinary differential equations in the frequency domain:

$$\begin{aligned} -\frac{d}{dx}[V] &= j\omega[L]\cdot[I] + [R]\cdot[I] \\ -\frac{d}{dx}[I] &= j\omega[C]\cdot[V] + [G]\cdot[V] \end{aligned} \tag{1}$$

Treating the n transmission lines as a $2n$-port system, we can derive from (1) the admittance matrix $[Y]$, which relates terminal voltages to terminal currents:

$$I_j = \sum_{k=1}^{2n} Y_{jk} V_k \tag{2}$$

The time domain counterparts become convolution relations:

$$i_j(t) = \sum_{k=1}^{2n} \int_0^t d\tau\, y_{jk}(t-\tau)\, v_k(\tau) \tag{3}$$

where y_{jk} is the inverse Fourier transform of $Y_{jk}(\omega)$. The terminal voltages and currents for any particular system can then be uniquely determined once the terminal conditions

$$[i(t)] = [f(v(t))] \tag{4}$$

are given. If all the terminations contain only linear elements, we can solve the problem in the frequency domain. Otherwise, iteration procedures are usually required for obtaining the solutions. The analyses presented in [1] and [9] are based on equations (3) and (4). Although their approaches are straightforward, there

exist problems that could possibly affect the efficiency of numerical computation. First of all, the parameter $y_{jk}(t)$ is equivalent to the current measured at port j with a voltage impulse excitation of unit amplitude at port k while ports other than k are short-circuited. Owing to strong reflections at the terminations, the duration of $y_{jk}(t)$ is usually long for slightly lossy transmission line systems, and even infinite for a lossless system. The long duration puts great demands on computer memory and execution time as required to perform convolution integrals of $[v(t)]$ and $[y(t)]$ during the iterative solution of nonlinear equations.

In order to overcome the disadvantage of using the parameters $\{y_{jk}\}$, the authors in [9] artificially insert a pair of complementary passive networks between the end of the transmission lines and the actual terminations. The purpose of that is to make the augmented linear network, which consists of the transmission line portion and the artificial network directly connected to the end of the transmission lines, a quasi-matched linear system so that the duration of the impulse responses for the augmented linear system can be effectively shortened. However, the other artificial network which is directly attached to the original load will contain negative resistors and hence may render the numerical solution unstable, especially when the transmission lines are lossless.

Instead of dealing with terminal voltage and current, we will analyze the transmission line system from the viewpoint of voltage waves. We choose the input and output waves at the terminal ports of the transmission lines as the variables of the problem as shown in Fig. 1. The parameters $\{B_j\}$ and $\{C_j\}$ are defined as follows:

$$B_j(\omega) = \frac{1}{2}\left[V_j(\omega) - Z_{0j}(\omega) \cdot I_j(\omega)\right] \tag{5}$$

$$C_j(\omega) = \frac{1}{2}\left[V_j(\omega) + Z_{0j}(\omega) \cdot I_j(\omega)\right] \tag{6}$$

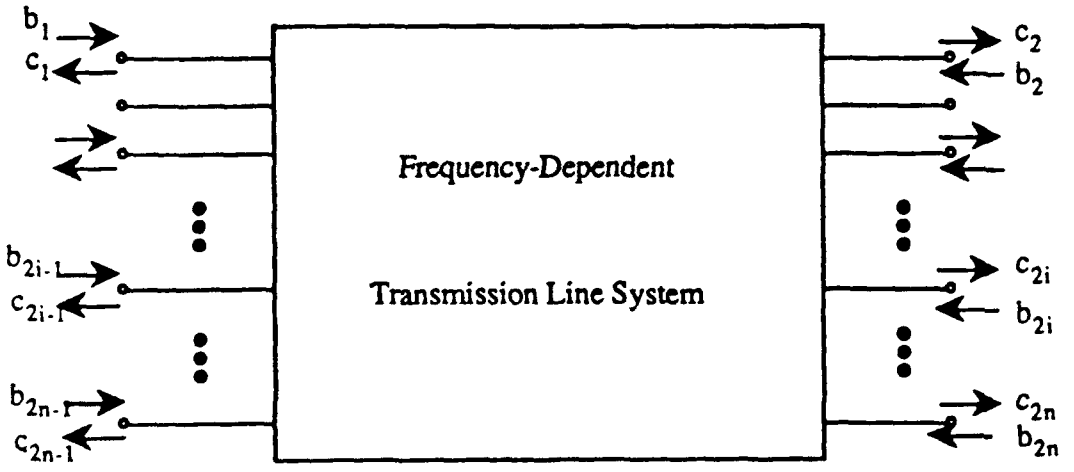

Figure 1. Linear multi-port network consisting of transmission lines.

where $Z_{0j}(\omega) = \sqrt{L_{jj}(\omega)/C_{jj}(\omega)}$ is the frequency-dependent characteristic impedance on line connected to port j. The linear dispersive transmission line system is thus characterized by a *scattering matrix* $[S_{ij}]$, i.e.,

$$\begin{bmatrix} C_1 \\ C_2 \\ C_3 \\ \vdots \\ C_{2n} \end{bmatrix} = \begin{bmatrix} S_{11} & S_{12} & S_{13} & \cdots & S_{1,2n} \\ S_{21} & S_{22} & S_{23} & \cdots & S_{2,2n} \\ S_{31} & S_{32} & S_{33} & \cdots & S_{3,2n} \\ \vdots & \vdots & \vdots & \ddots & \vdots \\ S_{2n,1} & S_{2n,2} & S_{2n,3} & \cdots & S_{2n,2n} \end{bmatrix} \begin{bmatrix} B_1 \\ B_2 \\ B_3 \\ \vdots \\ B_{2n} \end{bmatrix} \tag{7}$$

or

$$C_j(\omega) = \sum_{k=1}^{2n} S_{jk}(\omega) B_k(\omega) \qquad (k = 1, 2, \ldots, 2n) \tag{8}$$

It is easy to realize from the above equations that for all $j \neq k$, $S_{jk}(\omega)$ is equal to $2V_j(\omega)$ if all ports are loaded with their transmission line characteristic impedances and only a voltage source of amplitude 1 is applied at port k. This corresponds to impulse response or transfer functions in the time domain. If the coupling between individual transmission lines is weak, the system will be close to being perfectly matched. In this case we can conclude that the inverse Fourier transform of S_{jk}, denoted as $h_{jk}(t)$, will be of much shorter duration than $y_{ik}(t)$. Therefore we can effectively reduce the memory required to store the past values of h_{jk} and the time to compute the convolution integrals in

$$c_j(t) = \sum_{k=1}^{2n} \int_0^t d\tau \, h_{jk}(t-\tau) \, b_k(\tau) \tag{9}$$

without inserting any artificial networks.

We now have to solve $[b(t)]$ and $[c(t)]$ by incorporating the nonlinear boundary conditions of the problem. Specifically at port j, equations (5) and (6) lead to [8]

$$V_j(\omega) = B_j(\omega) + C_j(\omega) \tag{10}$$

and

$$2C_j(\omega) = V_j(\omega) + Z_{0j}(\omega) \, I_j(\omega) \tag{11}$$

By taking inverse Fourier transform on both sides of (10) and (11), we obtain their time domain counterparts:

$$v_j(t) = b_j(t) + c_j(t) \tag{12}$$

$$v_j(t) = 2c_j(t) - \int_0^t d\tau \, z_{0j}(t-\tau) \, f_j(v_j(\tau)) \tag{13}$$

where

$$z_{0j}(t) = \mathcal{F}^{-1}\left[Z_{0j}(\omega)\right]$$

Our problem will be solved in a time-marching fashion. At any instant t, the iteration procedure is as follows:

(i) Set up initial guess of $[b(t)]$. A reasonable choice is to take values from the previous time step.

(ii) Compute individual $\{c_j(t)\}$ using (9).

(iii) Apply standard nonlinear equation techniques such as Newton-Raphson method to (13) to solve for individual $\{v_j(t)\}$.

(iv) Obtain the next guess of $[b(t)]$ from the relation $b_j(t) = v_j(t) - c_j(t)$, and compare the guess with the previous one. If the error is above a pre-set tolerance, repeat steps (ii) to (iv) with the new guess.

For all practical purposes, we further divide these variables into two sets. The first corresponds to the source side of the transmission line system (Fig. 2), identified by odd-numbered subscripts, and the other corresponds to the load side (sourceless) with even-numbered subscripts (Fig. 3). The reason for doing so is based the following observations. The transfer functions linking $\{b_{2j}\}$ to $\{c_{2j+1}\}$ and $\{b_{2j+1}\}$ to $\{c_{2j}\}$ include time delay operators in order to account for the finite speed of propagation. In other words, $\{c_{2j+1}\}$ depend not on the present but the past values of $\{b_{2j}\}$ and the like for $\{c_{2j}\}$ on $\{b_{2j+1}\}$. As we carry out the iteration procedure step by step, the present values in one set will not interfere with those in the other. Therefore, the update of variables can be done simultaneously for any given time if parallel processing facilities are available.

In the next section we shall present the application of this method to a single dispersive line loaded by nonlinear impedance.

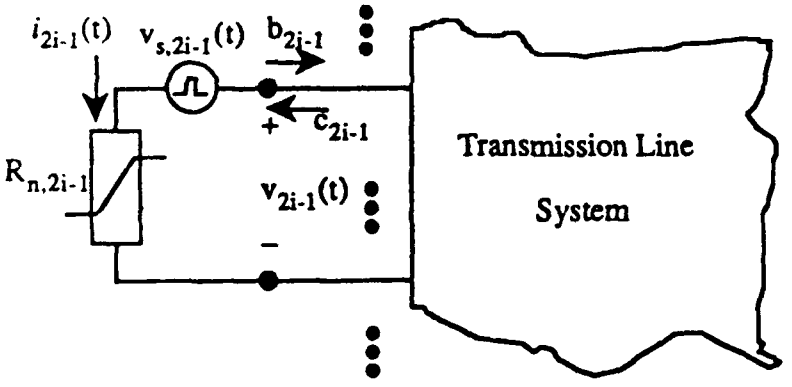

Figure 2. Odd-numbered ports (source side).

III. NONLINEARLY-LOADED DISPERSIVE TRANSMISSION LINE

Shown in Fig. 4 is a uniform dispersive transmission line of length l driven by a source $e_0(t)$ with a linear source resistance R_s at one end, and terminated by a nonlinear resistor R_n at the other end. The transmission line portion of this problem can be described in terms of the frequency dependent characteristic impedance $Z_0(\omega)$ and effective propagation constant $\beta(\omega)$. It can be shown that the frequency-domain *scattering matrix* is given as follows

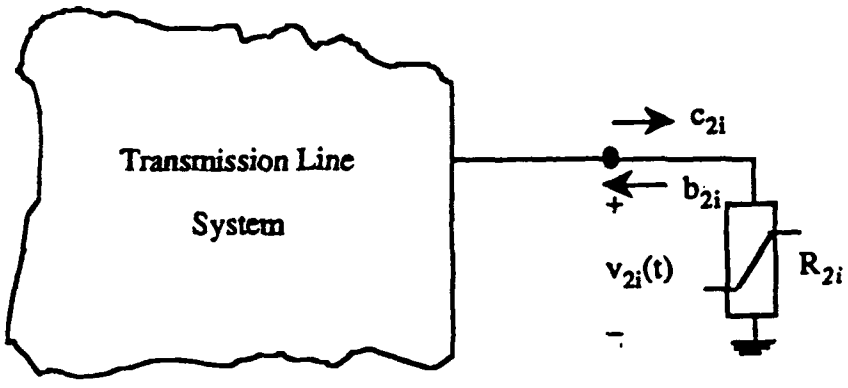

Figure 3. Even-numbered ports (load side).

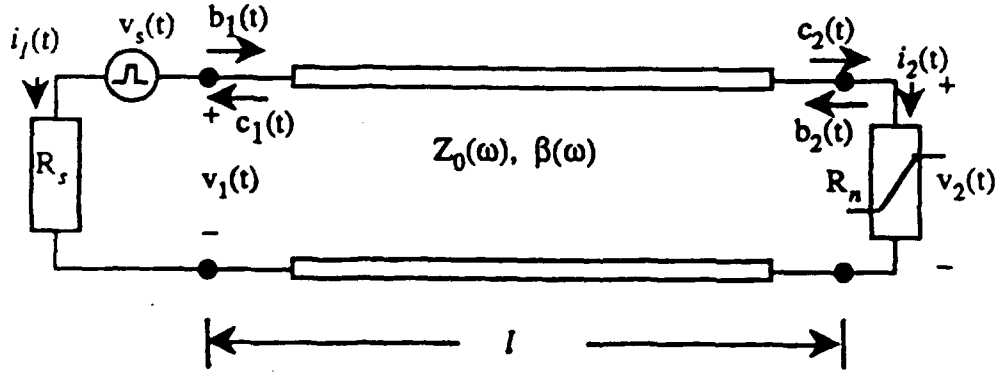

Figure 4. Nonlinearly loaded dispersive transmission line.

$$\begin{bmatrix} S_{11}(\omega) & S_{12}(\omega) \\ S_{21}(\omega) & S_{22}(\omega) \end{bmatrix} = \begin{bmatrix} 0 & e^{-j\beta(\omega)l} \\ e^{-j\beta(\omega)l} & 0 \end{bmatrix} \tag{14}$$

Noting that both S_{11} and S_{22} are zero for all time; therefore, we only need to consider S_{12} and S_{21}, which involve time delays. The simplicity of (14)

can be attributed to our definition of scattering matrix. As an example, we consider a microstrip line of width W. The substrate is of thickness h and has a dielectric constant ϵ_r. Numerous empirical formulas are available from the literature (see for example [13-15]). In this paper, we will use the following expressions to calculate the frequency dependence of microstrip line characteristic impedance and effective dielectric constant $\epsilon_e(\omega)$, which is defined from $\beta(\omega) = \omega\sqrt{\mu_0\epsilon_e\epsilon_0}$:

$$\epsilon_e(\omega) = \epsilon_r - \frac{\epsilon_r - \epsilon_e(0)}{1 + \frac{\epsilon_e(0)}{\epsilon_r}\left(\frac{\omega}{\omega_t}\right)^2} \tag{15}$$

$$Z_0(\omega) = \frac{\eta h}{W_e(\omega)\sqrt{\epsilon_e(\omega)}} \tag{16}$$

and the effective width $W_e(\omega)$ is governed by the equation

$$W_e(\omega) = W + \frac{W_e(0) - W}{1 + \omega/\omega_g} \tag{17}$$

where

$$\omega_t = \frac{\pi Z_0(0)}{\mu_0 h} \tag{18}$$

$$\omega_g = \frac{\pi c}{W\sqrt{\epsilon_r}} \tag{19}$$

and the low-frequency limits of ϵ_e and Z_0 are respectively

$$\epsilon_e(0) = \frac{\epsilon_r + 1}{2} + \frac{\epsilon_r - 1}{2} F(W/h) \tag{20}$$

with

$$F(W/h) = \begin{cases} (1 + 12h/W)^{-1/2} + 0.04(1 - W/h)^2, & \text{if } W/h \le 1 \\ (1 + 12h/W)^{-1/2}, & \text{if } W/h > 1 \end{cases} \tag{21}$$

and

$$Z_0(0) = \begin{cases} \frac{\eta}{2\pi\sqrt{\epsilon_e(0)}} \ln\left(\frac{8h}{W} + 0.25\frac{W}{h}\right), & \text{if } W/h \le 1 \\ \frac{\eta}{\sqrt{\epsilon_e(0)}}\left\{\frac{W}{h} + 1.393 + 0.667\ln\left(\frac{W}{h} + 1.444\right)\right\}^{-1}, & \text{if } W/h > 1 \end{cases} \tag{22}$$

Note that $W_e(0)$ in (17) is derived from (16) by substituting in $Z_0(0)$ and $\epsilon_e(0)$.

In this paper, we assume that the width W is equal to 0.508 mm and the depth and the dielectric constant of the substrate are equal to 0.216 mm and 10.2 respectively. It can be readily derived from the formulas that the effective permittivity in the low-frequency limit is equal to 7.46, and the high-frequency characteristic impedance is $Z_0(\infty) = 50.2\,\Omega$. The calculation of the impulse response function $h_{12}(t)\,(= h_{21})$, the inverse Fourier transform of $S_{12}(\omega)$, however, is not trivial. Because $\lim_{\omega\to\infty} S_{12}(\omega)$ does not approach 0, the inverse Fourier transform is singular. If numerical computations are not carried out with great care, the accuracy

would be questionable. In [16] a similar Fourier integral was calculated. The only difference is that the input is not an impulse function, and hence it is numerically integrable. The authors proposed using Taylor expansion method and the method of stationary phase for narrow-band input signals. But for other input waveforms a brute force numerical integration method was applied which proved to be very time-consuming. To overcome the difficulty of numerical integration once and for all, our approach is to separate the transfer function S_{12} into two parts, one that can be analytically inverted to an impulse function, and one that is well-behaved and integrable. The latter requires that the integrand approaches 0 as ω goes to infinity. This leads to a natural way of separation:

$$\begin{aligned} e^{-j\beta(\omega)l} &= \left(e^{-j\beta(\omega)l} - e^{-j\beta_\infty l}\right) + e^{-j\beta_\infty l} \\ &= e^{-j\beta_\infty l}\left\{\left[e^{-j(\beta(\omega)-\beta_\infty)l} - 1\right] + 1\right\} \end{aligned} \tag{23}$$

where $\beta_\infty = \omega\sqrt{\mu\epsilon_0\epsilon_r}$.

In (23), the factor $e^{-j\beta_\infty l}$ corresponds to a time delay of $\tau_r = l/(c\sqrt{\epsilon_r})$ and the inverse Fourier transform of 1 is an impulse function. Therefore, defining $h(t) = \mathcal{F}^{-1}\{e^{-j(\beta(\omega)-\beta_\infty)l} - 1\}$, we then have

$$h_{12}(t) = \delta(t-\tau_r) + h(t-\tau_r) \tag{24}$$

Now only $h(t)$ needs to be evaluated numerically. Because the kernel of this Fourier inversion has essentially a finite range of integration, the calculation becomes easier. The impulse response function for a 10 mm long microstrip line is shown in Fig. 5. Only a limited portion of $h_{12}(t)$ surrounds the impulse function. This is consistent with our claim that the impulse response has a very limited duration.

Because the scattering parameters h_{11} and h_{22} are zero, the input-output wave variable pair $\{b_j(t), c_j(t)\}$ are only linked through (12). The iterative solution to a single transmission line problem is therefore relatively simple. Once we finish calculating $v_j(t)$, iteration step (iv) will readily return the correct values for $b_j(t)$. There is no need to go back to step (i).

We first examine the response from a Gaussian pulse with an amplitude of 1.0 volts and a width of 10 ps measured at its half amplitude is used as the source. The source resistance R_s is 50 Ω. The load characteristics is fully described by the following equation:

$$i_2 = I_0\left[\exp\left(\frac{v_2}{0.025}\right) - 1\right] \text{ nA} \tag{25}$$

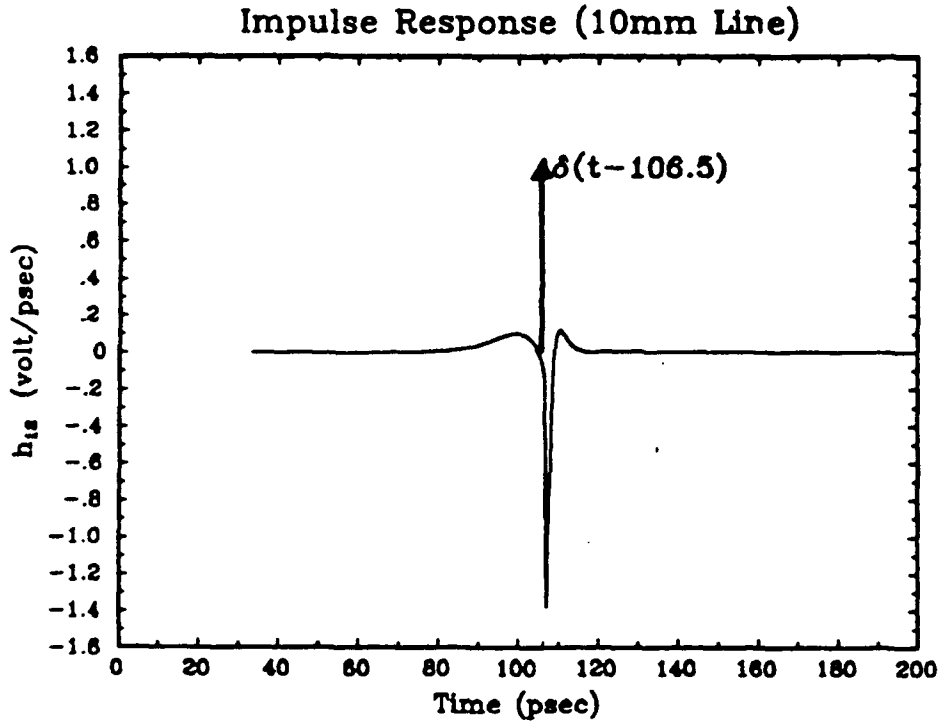

Figure 5. Impulse response $h_{12}(t)$.

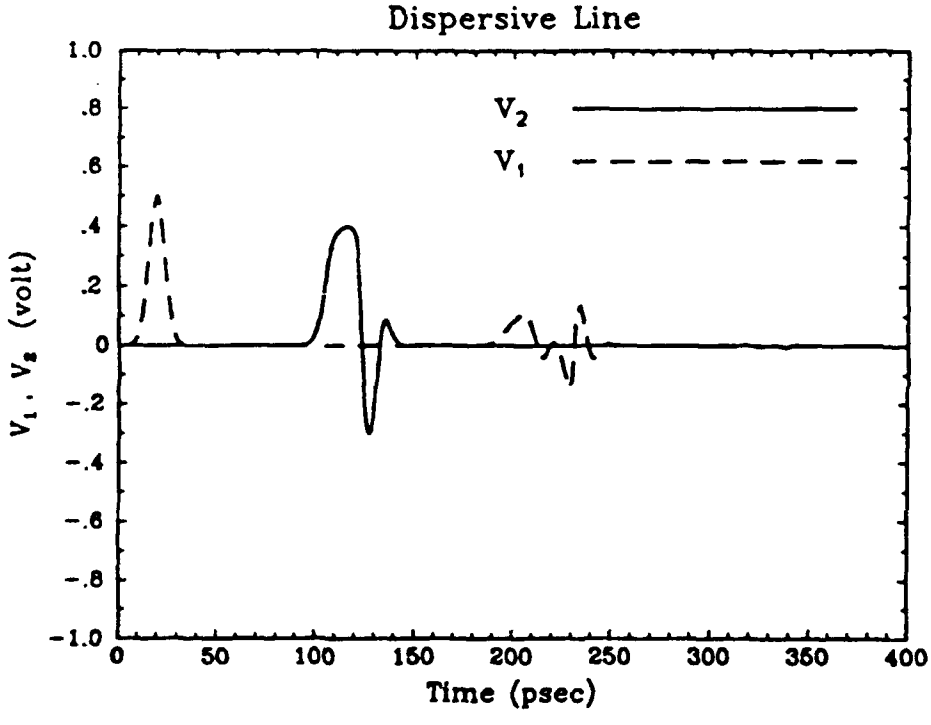

Figure 6. Terminal voltages vs. time at both the source end and the load end.

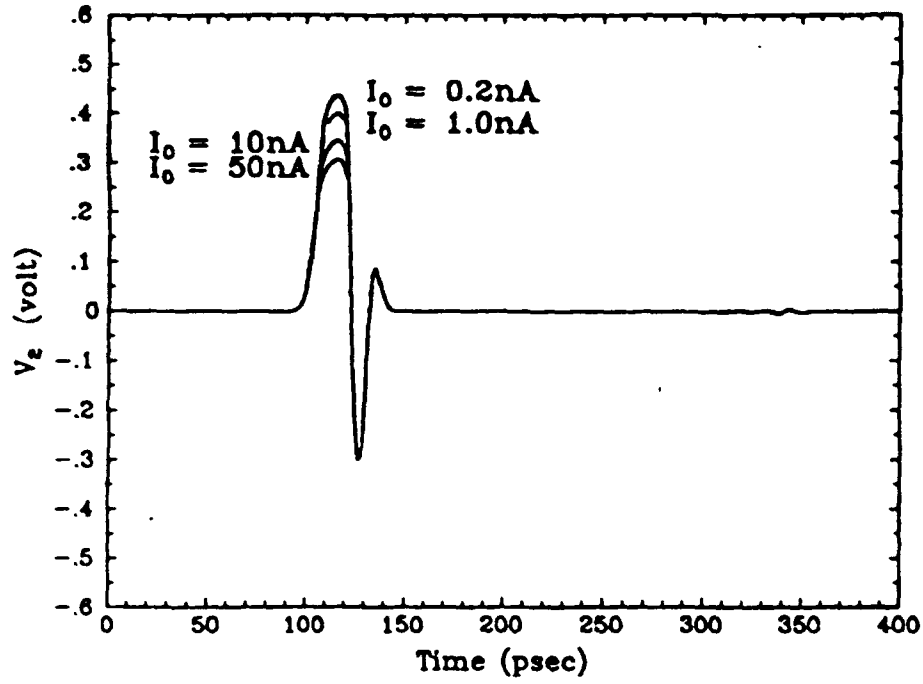

Figure 7. Load voltages as I_0 varies.

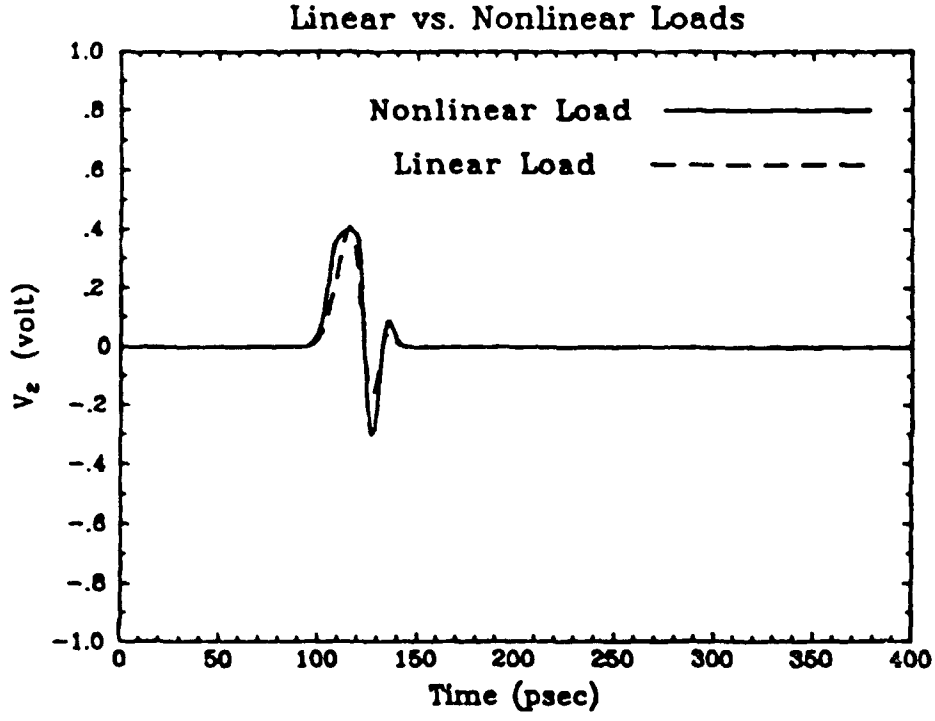

Figure 8. Load voltages for linear and nonlinear terminations.

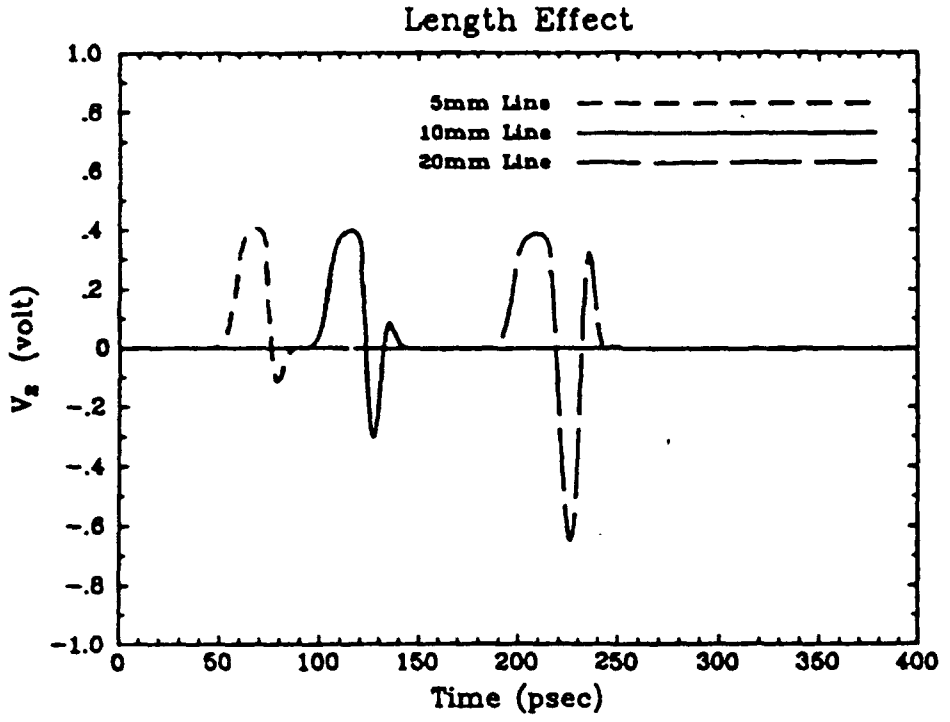

Figure 9. Load voltages for different line lengths.

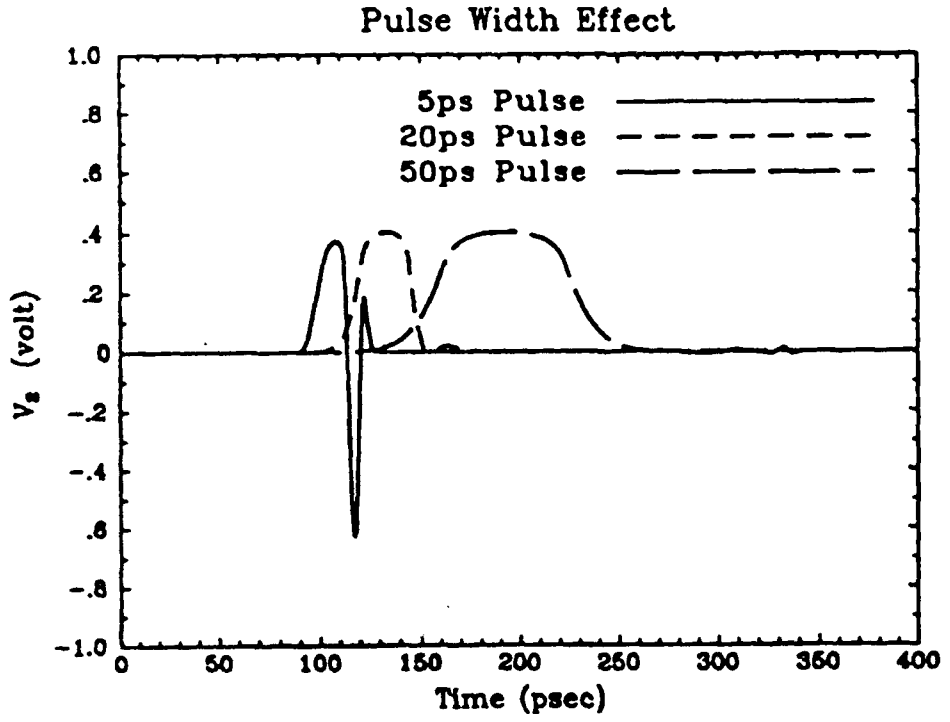

Figure 10. Load voltages for different pulse widths.

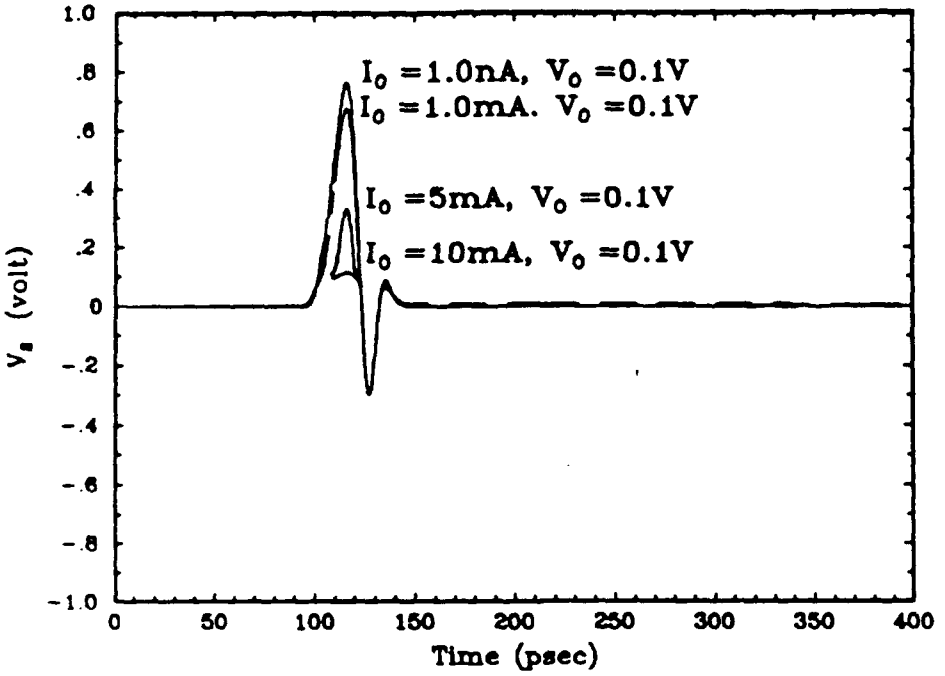

Figure 11. Load voltages for another type of nonlinear termination.

For the case $I_0 = 1.0$, the time responses at both ends are plotted in Fig. 6. The pulse has been broadened and the negative trailing edge is rather significant. In order to analyze what comes from dispersion of the transmission line and what comes from the load nonlinearity, we compared the plots of the load responses when I_0 is varied from 0.2 to 50.0 in (25), and when the load is a 50 Ω linear resistor. The results are depicted in Figs. 7 and 8. Apparently the nonlinearity contributes most to the broadening effect. The negative trailing edge originates from dispersion, but is enhanced by the nonlinear load. Since the load characteristics is similar to that of a typical diode, it behaves like an open circuit with respect to an incoming negative voltage wave. This gives rise to roughly twice the response compared to the one at the 50 Ω load, which is nearly matched to the transmission line. The large negative trailing edge also accounts for the extended ringing after it is reflected back to the source end.

In Fig. 9, the load end voltages for 5 mm and 20 mm lines are compared against the 10 mm line case. The number of zero crossings increases with length, as expected from the transmission line dispersion. Similar phenomenon is observed when shorter pulses are injected, as in Fig. 10. The centers of these pulses are intentionally separated to allow clearer comparison. It is interesting to note the similarity of the 5 ps pulse output and the 20 mm line output in Fig. 9.

We have also tested our iteration algorithm on another class of nonlinear loads

with i-v characteristics described as

$$i_2 = I_0\left[\tanh\left(\frac{v_2 - v_0}{0.025}\right) + 1.0\right] \tag{26}$$

Unlike the one described in (25), there is cap on the positive current. The result is that positive voltage has a larger amplitude, which is controlled by I_0, as shown in Fig. 11.

The time resolution used in all but the 5 psec pulse input case is 0.4 psec with a total of 1000 points. For the latter, the resolution is 0.2 psec and there are 2000 points. Because very limited portion of the impulse response $h_{12}(t)$ is significant, the actual number of points involved in the convolution integral is far lower. We used the Newton-Raphson iteration procedure for the nonlinear equation (13). On a VAX Station 3500, the testing cases take about 4 to 27 seconds of CPU time to generate the solutions with 1000 points. The large variation in computation times is due to different convergent rates for different types of nonlinearity.

IV. CONCLUSIONS

A new method for the transient analysis of a frequency-dependent transmission line system terminated with nonlinear loads has been presented. This method is not only effective for saving the CPU time required for solving nonlinear transient problems, but is also compact and natural in form. Our generalized scattering matrix approach is closely tied to the concept of waves. Therefore, no extended reflection arises as a result of artificial boundary conditions as can occur with the admittance matrix method, and duration of the impulse responses for the waves in the transmission line system is very limited. This is the key to reducing the amount of computation time and memory.

The detailed procedure for solving this kind of nonlinear transient problem is given through an analysis of a nonlinearly-loaded microstrip transmission line with linear source resistance. Extension of this approach to multiple transmission line systems with nonlinear source and terminations is being studied and will be reported in future work.

ACKNOWLEDGMENTS

This paper was supported by the ARO Contract DAAL03-88-5-0057, NSF Grant 8620029-ECS, the Joint Service Electronics Programs under the Contract DAAL03-86-K-0002, and the Digital Equipment Corporation.

The Editor thanks S. Ali and two anonymous Reviewers for reviewing the paper.

REFERENCES

1. Liu, T. K., and F. M. Tesche, "Analysis of antennas and scatterers with nonlinear loads," *IEEE Trans. Antennas Propagat.*, Vol. AP–24, 131–139, 1976.
2. Gu, Q., J. A. Kong, and Y. E. Yang, "Time domain analysis of nonuniformly coupled line systems," *J. Electro. Waves Applic.*, Vol. 1, 109–132, 1987.
3. Nakhla, M. S., and J. Vlach, "A piecewise harmonic balance technique for determi-

nation of periodic response of nonlinear systems," *IEEE Trans. Circuits & Systems*, Vol. CAS–23, 85–91, 1976.
4. Rizzoli, V., V. Lipparini, and E. Marazzi, "A general purpose program for nonlinear microwave circuit design," *IEEE Trans. Microwave Theory Tech.*, Vol. MTT–31, 762–770, Sept. 1983.
5. Gilmore, R. J., and F. J. Rosenbaum, "Modelling of nonlinear distortion in GaAs MESFETS," *IEEE 1984 Int. Microwave Symp. Dig.*, 430–431, June 1984.
6. Gilmore, R., "Nonlinear circuit design using the modified harmonic balance algorithm," *IEEE Trans. Microwave Theory Tech.*, Vol. MTT–34, No. 12, 1294–1307, Dec. 1986.
7. Merewether, D. E., and T. F. Ezell,"The interaction of cylindrical posts and radiation-induced electric field pulses in ionized media," *IEEE Trans. Nuclear Sci.*, Vol. NS–21, 4–13, 1974.
8. Schuman, H., "Time-domain scattering from a nonlinearly loaded wire," *IEEE Trans. Antennas Propag.*, Vol. AP–22, 611–613, 1974.
9. Djordjevic, A. R., T. K. Sarkar, and R. F. Harrington, "Analysis of transmission lines with arbitrary nonlinear terminal networks," *IEEE Trans. Microwave Theory Tech.*, Vol. MTT–34, No. 6, 660– 666, June 1986.
10. Caniggia, S., "EMC design of digital systems using macromodelling procedures for integrated circuits and their interconnections," *Proc. EMC Symp.*, 465–470, 1983.
11. Schutt-Aine, J. E., and R. Mittra, "Scattering parameter transient analysis of transmission lines loaded with nonlinear terminations," *IEEE Trans. Microwave Theory Tech.*, Vol. MTT–36, 529–536, 1988.
12. Collin, R. E., *Field Theory of Guided Waves*, McGraw-Hill Book Company Inc., 1960.
13. Pramanick, P., and P. Bhartia, "An accurate description of dispersion in microstrip," *Microwave J.*, 89–93, Dec. 1983.
14. Gupta, K. C., *Microstrip Lines and Slotlines*, Artech House, Dedham, Massachusetts, 1979.
15. Kirchning, M., and R. H. Jansen, "Accurate wide-range design equations for the frequency-dependent characteristic of parallel coupled microstrip lines," *IEEE Trans. Microwave Theory Tech.*, Vol. MTT–32, 83–90, Jan. 1984.
16. Veghte, R., and C. A. Balanis, "Dispersion of transient signals in microstrip transmission lines," *IEEE Trans. Microwave Theory Tech.*, Vol. MTT–34, No. 12, 1427–1436, Dec. 1986.

Qizheng Gu was born in Jiangsu, China. He graduated from Fudan University, Shanghai China in 1960. From 1960 to 1962, he worked on automatic control systems at Shanghai Designing Institute of Machinery and Electrical Engineering, China. In 1962, he joined the Department for Research and Development at Shanghai Xinhua Radio Factory, where he was engaged in research of microwave systems and circuits. Since October 1982, he has been a senior engineer and the Deputy Director of the Department. Between 1983 and 1987, he was a visiting scientist in the Research Laboratory of Electronics, Massachusetts Institute of Technology. He is a member of the Shaghai Electronics Association Council and the Microwave Committee of the Chinese Institute of Electronics.

Ying-Ching Eric Yang was born in Taiwan in 1959. He received his B.S.E.E. degree from National Taiwan University in 1981 and the M.S. and E.E. degrees from the Massachusetts Institute of Technology in 1985 and 1986, and is currently working toward his Ph.D. degree. From 1981 to 1983 he served in the R.O.C. Navy as an instructor. Since 1983 he has been with the department of electrical engineering and computer science and the Research Laboratory of Electronics of the Massachusetts Institute of Technology, where he worked as a Research Assistant and a Teaching Assistant. He was an IBM Graduate Fellow during the academic year 1986–87. His reseach interest is in the time-domain

electromagnetic wave propagation within microelectronic integrated circuits. Mr. Yang is a member of the IEEE and Sigma Xi.

Jin Au Kong is Professor of Electrical Engineering and Chairman of Area IV on Energy and Electromagnetic Systems in the Department of Electrical Engineering and Computer Science at the Massachusetts Institute of Technology, Cambridge, Massachusetts. His research interest is in the field of electromagnetic wave theory and applications. He is the author of *Electromagnetic Wave Theory* (Wiley, 1975, 1986), coauthor of of *Applied Electromagnetism* (Brook/Cole, 1983 PWS, 1987) and *Theory of Microwave Remote Sensing* (Wiley, 1985), and Editor of *Research Topics in Electromagnetic Wave Theory* (Wiley, 1981), Chief Editor of the Elsevier book series on Progress in Electromagnetics Research (PIER) and the Wiley Series in Remote Sensing.